PROCUREMENT EXECUTIVE, MINISTRY OF DEFENCE

AERONAUTICAL RESEARCH COUNCIL

CURRENT PAPERS

Film Cooling Effectiveness from Rows of Holes under Simulated Gas Turbine Conditions

by

M. R. Smith, T. V. Jones and D. L. Schultz

Oxford University

FILM COOLING EFFECTIVENESS FROM ROWS OF HOLES
UNDER SIMULATED GAS TURBINE CONDITIONS
- by -
M.R. Smith, T.V. Jones and D.L. Schultz
Oxford University

SUMMARY

Experiments are reported in which film cooling tests are carried out using coolent injection through rows of discrete holes. A shock tunnel is used to provide a transient mainstream flow at stagnation temperatures of 500°K, 1000°K and 2000°K. Wall heat transfer rates are measured with and without coolant injection using thin film gauges. Mainstream Mach numbers of 0.2, 0.5 and 0.7 are employed. Mach numbers, Reynolds numbers, gas-to-wall temperature ratios and flow temperatures typical of those found in gas turbines are thus within the range of the experimental conditions.

The experimental results are analysed using the boundary layer film cooling model parameter $\bar{x}$ and the mass and momentum flux ratios as correlating parameters. The latter gives good correlation of the experimental data, and a useful comparison with data obtained by other workers under different conditions. The correlated data may also be used as a prediction for film cooling in any situation, and as a test for new theoretical models of the film cooling process.

List of Contents

1. INTRODUCTION

Research on film cooling has been stimulated recently by the demand for increased turbine entry temperatures as a means of increasing the thrust available from a given engine core. Wieghardt (1) first studied the subject of gas injection to alter heat transfer or fluid dynamics. He investigated the reverse problem, that of deicing aircraft wings with slot injection of heated air. There is also a substantial literature on the application of film cooling to supersonic and hypersonic vehicles usually employing slots or louvres, (2) and (4). Similar techniques are employed in the cooling of combustion chambers and wind tunnel nozzles but it is only fairly recently that attention has been directed towards the film cooling of the external surfaces of turbine blading. Such blades have been cooled by through-flow systems since about 1951 (3) and subsequently film cooling has been employed in addition. Goldstein (4) has reviewed developments in film cooling and this reference should be consulted for a complete survey of the field. The general scheme employed for air supply and ejection from a blading system is illustrated in Fig.1. Several features which distinguish this form of cooling may be recognised in this illustration. Structural considerations, particularly in the rotor blading demand the use of discrete holes which cannot be located at close centre spacings. The ejected gas cannot therefore be considered as providing a protective cool layer, as might be the case with a tangential slot, but must act by lowering the mean temperature in the boundary layer, after a mixing process. This action may be contrasted with that in transpiration cooled surfaces where cooling is achieved over the region of coolant ejection. The phenomena which control this mixing process in the case of discrete holes will therefore be of prime importance in maintaining effective cooling, both close to and remote

from the injection holes, and techniques for the prediction of cooling

effectiveness must be valid for a wide range of axial distances relative

to hole diameter. Coolant air is normally bled from the final stage

of the compressor and supplied to the blades via their roots, passing

through internal passages where additional total blade cooling is

achieved, and is finally ejected through holes distributed over the

blade surface. Information on the effect of coolant to-free-stream

pressure ratio on cooling effectiveness is therefore expected to be

important in predicting performance in a system in which the free

stream stagnation pressure can equal the coolant stagnation pressure.

The present report deals with the results of experiments

designed to provide information on the efficiency of arrays of discrete

holes in reducing the heat transfer rate to plane surfaces. The tests

have been conducted in short duration facilities previously described,

(5), (6) and (7), which enable heat transfer rates to be determined

with thin film gauges (8). Three flow Mach numbers, 0.2, 0.5 and 0.7

were used as representative of engine conditions with Reynolds numbers

in the range 3×10^6 to 3×10^8 per metre. Three stagnation tempera-

tures, $2000^\circ K$, $1000^\circ K$ and $500^\circ K$ were employed to give free-stream to

wall temperature ratios of 6.6, 3.3 and 1.6. This variation in free

stream properties was found to be important in gaining an understanding

of the fluid dynamics of the injection process.

The results of the experiments are analysed using both the slot-

injection cooling parameter $\bar{x}$ and the mass and momentum flux ratios,

in an effort to determine which parameter governs the processes

involved, and so eventually to predict film cooling effectiveness in

any situation. The choice of such a governing parameter also allows

comparison with the results of other workers, who have usually obtained

their data under conditions very different to those employed here.

The comparison thus provides a check on both the data and the corre-

lating parameter.

2. APPARATUS AND EXPERIMENTAL TECHNIQUE

The apparatus and experimental technique used are those employed by Jones and Schultz (5), whose paper gives a full description of the technique which is only briefly outlined in this report. A reflected-shock tunnel was used to provide a hot nitrogen flow of duration 5-10ms. through the nozzle, (Fig.2(a)), fitted with plane glass schlieren side windows, a flat brass liner on the upper surface and a contoured brass liner on the lower surface. The contoured liner had a straight section which produced a parallel subsonic region. In this region, in the top liner, were the coolant injection holes and the thin film gauges used to measure heat transfer. The voltage signal from the thin film heat transfer gauges corresponds to the rise in surface temperature; this was converted to a heat transfer rate signal by means of an electrical analogue circuit. The heat transfer rate was then measured directly. The thin film and analogue techniques are fully described in Ref.(8). A "floor plan" showing the positions of the downstream gauges relative to the injection holes is illustrated in Fig.2(b). It can be seen that the gauges produce an average reading in the spanwise (y) direction since they are much wider than the holes; in fact they "see" the effect of four holes in the double row case and two holes in the single row case. However each gauge produces a single point reading in the x (flow) direction. The general arrangement and dimensions of the injection holes are shown in Fig.2(c).

The static pressure of the flow in the working section and at the throat was measured using quartz piezo-electric pressure transducers mounted behind 1mm. diameter pressure tappings in the lower liner. The total pressure was measured with a similar transducer mounted in the end of the shock tube.

The total temperature of the flow was calculated from measurements of the speed of the shock in the shock tunnel. The coolant used in the experiments was nitrogen, at room temperature, which reached the injection holes through a short passage leading from a plenum chamber immediately above the nozzle. The coolant flow was initiated by a solenoid operated pin which ruptured a plastic diaphragm, thus connecting the plenum chamber with the injection holes. The flow of coolant gas was initiated a short time before the main flow to enable a stable flow system to be established. The rate of flow of the coolant was measured by monitoring the rate of fall of pressure in the plenum chamber with a piezo-electric pressure transducer.

3. QUANTITIES DERIVED FROM THE EXPERIMENTAL RESULTS

The basic quantities which are used in the analysis of the experimental data are as follows:-

(1) The ratio of heat transfer rate with injection to that without injection, $\dfrac{\dot{q}_i}{\dot{q}_o}$. The heat transfer rate in the absence of cooling, $\dot{q}_o$, was measured for each gauge on a series of runs without injection. An average $\dot{q}_o$ value was calculated for each gauge. The heat transfer rate with coolant injection $\dot{q}_i$ was measured. $\dot{q}_i$ was then normalised so that the data upstream of the holes was the same as for the runs without coolant injection. In this manner errors due to flow variations which may occur in the shock tunnel from run to run were minimised.

(2) The injection mass flux, $\rho_{si} u_i$. This was calculated from the rate of fall of pressure in the plenum chamber, which, assuming that the flow from the chamber was isentropic (at least for the short run time considered), is related to the

mass flow rate by the expression

$$\frac{dP_{Ti}}{dt} = \frac{\gamma \dot{m} R T_{Ti}}{V_i}$$

Since the mass flow rate $\dot{m}$ is $\rho_{si} u_i N a_h$,

$$\rho_{si} u_i = \frac{V_i}{N a_h a_i^2} \frac{dP_{Ti}}{dt}$$

where $\rho_{si} u_i$ is an average value over all the area of all the holes; it should be noted that it is not necessary to intro-duce a discharge coefficient at this stage.

(3) The free stream mass flux $\rho_{s\infty} u_\infty$. The volume flow rate through a sonic throat from a reservoir is given by

$$V = \left(\frac{2}{\gamma+1}\right)^{\frac{\gamma+1}{2(\gamma-1)}} a_o A^* = 0.579 a_o A^* \text{ (for } \gamma = 1.4)$$

The mass flow rate through the nozzle is thus

$$\rho_{s\infty} u_\infty A_N = 0.579 \, \rho_{T\infty} a_{T\infty} A^*$$

Thus $\rho_{s\infty} u_\infty = 0.579 \dfrac{A^*}{A_N} \dfrac{\gamma P_{T\infty}}{a_{T\infty}}$

$\dfrac{A^*}{A_N}$ is defined by the geometry of the nozzle, $P_{T\infty}$ was measured for each run and $a_{T\infty}$ may be derived directly from the stagnation temperature of the flow (calculated from measurements of the shock Mach number in the shock tube). Thus $\rho_{s\infty} u_\infty$ may be calculated.

(4) Injected flow velocity at hole exit, u_i. If it is assumed that the pressure of the injected gas P_{si} at the exit of the coolant holes is approximately equal to $P_{s\infty}$, (it will not in general be exactly equal to $P_{s\infty}$ as the main stream will recover some pressure against the emerging coolant jet) then

$$\frac{\rho_{Ti}}{\rho_{si}} = \left(\frac{P_{Ti}}{P_{s\infty}}\right)^{\frac{1}{\gamma}}$$

and since $\rho_{si}u_i = \dfrac{V_i}{Na_ha_i^2} \dfrac{dP_{Ti}}{dt}$ and $P_{Ti} = \rho_{Ti}RT_{Ti}$;

$$u_i = \rho_{si}u_i \times \dfrac{\rho_{Ti}}{\rho_{si}} \times \dfrac{1}{\rho_{Ti}}$$

$$= \dfrac{V_i}{Na_ha_i^2} \dfrac{dP_{Ti}}{dt} \times \left(\dfrac{P_{Ti}}{P_{s\infty}}\right)^{\tfrac{1}{\gamma}} \times \dfrac{RT_{Ti}}{P_{Ti}}$$

Thus:

$$u_i = \dfrac{V_i}{\gamma Na_h} \cdot \dfrac{1}{P_{Ti}} \dfrac{dP_{Ti}}{dt} \left(\dfrac{P_{Ti}}{P_{s\infty}}\right)^{\tfrac{1}{\gamma}}$$

It is of interest at this point to note that the value

of $\rho_{si}u_i$ given by the measurement of $\dfrac{dP_{Ti}}{dt}$ will not agree

with a value given by a calculation based on $\dfrac{P_{Ti}}{P_{si}}$ (which

is assumed to equal $\dfrac{P_{Ti}}{P_{s\infty}}$). The ratio of these two values

is the discharge coefficient C_D. C_D has been calculated

for most of the experiments as shown in Fig.3 and found

to be virtually constant for all tests except those with

the very smallest pressure ratios where the possible

errors in the pressure measurement are much greater. The

value of C_D was approximately 0.7, for $\dfrac{P_{Ti}}{P_{s\infty}}$ greater than

about 1.2 for all Mach numbers and hole geometries.

(5)   The free stream velocity u_∞. Measurements of the area

ratio of the nozzle were used to provide values of M_∞

and $\dfrac{U_\infty}{a_o}$ directly from flow tables. The value of a_o is

known from measurements of the shock speed, as already

mentioned.

The free stream Mach number M_∞ can alternatively be found

from the pressure ratio $\dfrac{P_{s\infty}}{P_{T\infty}}$. However, any errors in

pressure measurement can make this method less accurate,

especially at low subsonic Mach numbers, and so the Mach

number defined by the area ratio was used for the purposes of analysis.

Combinations of all the above quantities enabled the parameters such as I, J, K and $\bar{x}$, which are used in the correlation of the data, to be calculated.

4. DISCUSSION OF EXPERIMENTAL DATA

(a) Film Cooling Effectiveness

A commonly used method for the correlation of film cooling experiments has been to plot the film cooling effectiveness η against some parameter indicating the rate of coolant injection. The effectiveness is usually defined by

$$\eta = \frac{T_{aw} - T_{T\infty}}{T_{Ti} - T_{T\infty}} \ .$$

It is a measure of the cooling property of the film, insofar as

$$\eta = 1 \text{ when } T_{aw} = T_{Ti} \quad \text{and} \quad \eta = 0 \text{ when } T_{aw} = T_{T\infty}$$

In the present work, heat transfer rate without coolant injection $\dot{q}_o$ and heat transfer rate with injection, $\dot{q}_i$ have been measured. The ratio of these quantities is used instead of effectiveness. However, since $\dot{q}_o = h_o (T\infty - T_w)$ where h_o is the heat transfer coefficient without injection, and $\dot{q}_i = h_i (T_{aw} - T_w)$ where h_i is the heat transfer coefficient when injection is present,

$$\frac{\dot{q}_i}{\dot{q}_o} = \frac{h_i (T_{aw} - T_w)}{h_o (T_{T\infty} - T_w)}$$
. If the commonly used assumption is now made, (9),

that $h_i = h_o$, and it is noted that in the present experiment

$T_{Ti} \approx T_w$ (room temperature), then

$$\frac{\dot{q}_i}{\dot{q}_o} = \frac{T_{aw} - T_w}{T_{T\infty} - T_w} \approx \frac{T_{Ti} - T_{aw}}{T_{Ti} - T_{T\infty}} \approx 1 - \eta$$

The parameter $\dfrac{\dot{q}_i}{\dot{q}_o}$ used here is thus easily linked with film cooling

effectiveness, η.

(b) <u>The Effect of Coolant-to-Free-Stream Pressure Ratio</u>

During the course of the present work, the results obtained were first plotted in the form shown in Fig.4 as $\dfrac{\dot{q}_i}{\dot{q}_o}$ against $\dfrac{x}{d}$.

The cooling is generally most efficient near the injection position (small $\dfrac{x}{d}$) and decreases (increasing $\dfrac{\dot{q}_i}{\dot{q}_o}$) at larger distances downstream. The cooling effect at all positions is generally improved by increasing the injection-to-free-stream total pressure ratio $\dfrac{P_{Ti}}{P_{T\infty}}$. The exception to this is at high injection-to-free-stream total pressure ratios, when at positions near the holes the cooling effect is not as good as might be expected. The reasons for this, and the nature of the flow may be more readily seen from plots of $\dfrac{\dot{q}_i}{\dot{q}_o}$ against $\dfrac{P_{Ti}}{P_{T\infty}}$ for single values of $\dfrac{x}{d}$, as in Figs. 5 to 10.

Cooling is seen to commence when the total pressure of the injected gas is equal to the static pressure in the working section and the effect increases in general as the coolant pressure is increased. At downstream positions close to the coolant injection holes the effectiveness decreases if the injectant total pressure is increased too far as may be seen in Fig. 5(a). This reduction in effectiveness apparently arises because the coolant gas may, at high injection pressures penetrate the boundary layer and enter the mainstream. Further downstream, however, this effect is not noticed (Figs.5(b) and (c)), presumably because

mixing has taken place. The change in the trajectory of the jets as the coolant pressure is increased can be seen in the shadowgraphs, Plate 1.

At a mainstream Mach number of 0.2 the increase in cooling effectiveness with injectant pressure is, as can be seen in Fig.6 much more rapid than at higher Mach numbers. The development of lift off in this instance can be traced in Plate 2. Raising the mainstream Mach number to 0.7 had the opposite effect, as seen in Fig.7 and Plate 3 where lift-off is hardly apparent.

Changing the injection angle from $90°$ to the main stream to $30°$ to the mainstream also had the effect of making the onset of cooling more abrupt with increasing injectant pressure. The lift-off effect appeared to be slightly less severe (Fig.8 and Plate 4). It should also be noted that in this case two different spacings of the rows of holes were used, $\frac{r}{s} = \frac{\sqrt{3}}{2}$ (points σ and $\bullet$) and $\frac{r}{s} = \frac{\sqrt{3}}{4}$ (points o and $\bullet$). However, this variation seemed to have little if any effect and so the results for both spacings are plotted on the same graphs.

The other variation of the geometry was to use only one row of holes instead of two. As shown in Figs.9 and 10, this made the lift-off effect much more severe. It was now apparently easier for the mainstream flow to penetrate between the jets of coolant; indeed possibly the coolant jets were actually inducing the mainstream between them to flow towards the wall. This would account for some of the results which show that in extreme cases the heat transfer rate to the wall immediately behind the holes was even greater than when no injection was present. The

lift-off effect was much more severe than for the case of two rows
of holes, at both the 30° and 90° injection angles, as can be
seen in Plates 5 and 6.

It should be noticed at this stage that in plotting the
heat transfer rate data against $\frac{P_{Ti}}{P_{T\infty}}$, data collected with two dif-

ferent values of the free stream stagnation temperature, and at

two different pressure levels, have been included in the same

figures, and for a given M_∞ correlate well. The reasons for

this will be discussed later in the paper.

(c) Correlation of the Data

The most usual method of correlation of data from three-

dimensional film cooling experiments in the past has been to plot

the film cooling effectiveness η against the blowing rate I, (9)

and (10). Examination of Fig.11(a) reveals that this treatment

does not correlate the results of the present work at all well.

There is a discrepancy between the two sets of data obtained at

different free stream temperatures. Changing from the mass flux

ratio to the momentum flux ratio J meets with much more success,

as shown in Fig.11(b). Here results obtained at different free

stream temperature levels, Mach numbers and pressure levels are

all correlated quite well.

An alternative parameter against which to correlate heat

flux ratio is the energy flux ratio K, as shown in Fig.11(c).

However it appears to produce only a slight improvement on the

correlation obtained with the parameter J.

To show more clearly the relative improvement to

be gained from using J or K, results obtained at all Mach numbers,

temperature levels and pressure levels are plotted against loga-

rithmic scales of I, J and K in Fig.12, for both the 1 row, 90°

and 2 rows, 90° geometries.Comparison of Figs.12(b) and 12(c)

shows that plotting against the parameter K produces little if

any significant improvement over plotting against J. However

both these parameters offer a large improvement in correlation

over that obtained using I in Fig.12(a).

It was therefore decided to plot all the data against J.

Figs.13 to 17 show mean curves obtained from plots of data

at all Mach numbers temperature and pressure levels for each

geometry. Figs.18 and 19 are included to illustrate the degree

of scatter of data points about these mean curves.

The success of J as a correlating parameter is one explana-

tion for the usefulness of $P_{Ti}/P_{T\infty}$ in the initial analysis of the

data. $\dfrac{P_{Ti}}{P_{T\infty}}$ is indeed equivalent to $\dfrac{\rho_{si} u_i^2}{\rho_{s\infty} u_\infty^2}$ at a fixed free stream

Mach number and gave excellent correlation at each separate Mach

number, including correlation of results obtained at different

temperature and pressure levels. As expected the pressure ratio

did not correlate results obtained at different Mach numbers as

shown in Fig.20. $\dfrac{P_{Ti}}{P_{s\infty}}$ was also tried as a correlating parameter; in

spite of its correlation of the onset of cooling, the curves cor-

responding to the different Mach numbers separated as the blowing

pressure increased.

It should be noted here that the use of a simple pressure

ratio $\dfrac{P_{Ti}}{P_{T\infty}}$ as a correlating parameter has advantages for the engine

designer since it is likely that this ratio will be known with

greater accuracy than the mass flux ratio.

(d) Comparison with the Data of Other Workers

Having chosen a parameter which gives a good correlation of

the present data, it is desirable to compare the present

results with those of other experimenters. This is particu-

larly interesting because most of the available data has been obtained under conditions completely different from those of the present tests.

The data for single row injection at an angle of 30° has been chosen for comparison because there is more data comparable with this than with any of the other geometries.

Figs.21, 22 and 23 show the present data points with lines taken from Goldstein et al (10) and Liess and Carnel (11).

The present results were obtained under compressible flow conditions at a Mach number of 0.5 and stagnation temperatures $1000^\circ K$ and $500^\circ K$, with cold gas injection.

The measurements of Goldstein et al (10) were made under incompressible, room-temperature mainstream conditions with injection of air heated to a temperature $55^\circ C$ higher than that of the mainstream. The injection geometry was a row of holes angled at 35° to the mainstream with a spacing-to-diameter ratio $(\frac{s}{d})$ of 3.0. The conditions of Liess and Carnel (11) were similar except that the injectant gas was heated to $120^\circ C$ and the spacing-to-diameter ratio was 2.22.

Taking these large variations in experimental technique into consideration, the correlation of the data obtained is convincing. The results are all of the same form, only showing variations in

the level of cooling effectiveness. These variations are
expected, however, because the effectiveness will be higher when
the holes are closer together.

5. COMPARISON WITH SIMPLE 2-DIMENSIONAL FILM COOLING THEORY

The above correlations of cooling effectiveness with injec-
tion momentum flux do not incorporate any form of scaling with
distance downstream of the injection holes. This scaling has
been achieved in the past (see (4) for references) but only in
theories describing cooling experiments with injection through
slots rather than through discrete holes. These theories have
been derived from an energy balance in the boundary layer, and
depend to some extent on the two-dimensionality of the flow.
The proposed correlations usually take the form $\eta = A(\bar{x} + B)^{-0.8}$
where A and B are constants and $\bar{x} = \frac{x}{IS}\left(Re_i \cdot \frac{\mu_i}{\mu_\infty}\right)^{-\frac{1}{4}}$. S is the
slot height and I is the "blowing rate" parameter $\frac{\rho_{si}u_i}{\rho_{s\infty}u_\infty}$ mentioned
above.

The present results have been put in this form by postu-
lating a slot, whose height is such as to give the same ejection
area per unit width as the single or double rows of holes.

Having calculated the effective slot height in this way,
the cooling effectiveness, or $\frac{\dot{q}_i}{\dot{q}_o}$ may be plotted as a function of
$\bar{x}$ and compared with a simple slot theory, for example that of
Stollery and El-Ehwany (12) as shown in Figs.24 to 27. It is
apparent that for large $\bar{x}$ (large x or small I) the holes are
nearly as effective as a slot. The difference grows, however,
as $\bar{x}$ is reduced, indicating the presence of much more mixing
of the free stream and coolant gas in the hole-injection case.
At values of $\bar{x}$ below a certain limit (much smaller for 2 rows
than for 1 row) the experimental results show a sudden decrease

in cooling effectiveness, thought to be due to the phenomenon of "lift-off" already described.

As shown in Fig.28 an increase in heat transfer rate due to a lift-off effect is not observed when a slot is used to inject the coolant, as the hot mainstream is not able to penetrate the jet of coolant and increase the heat transfer rate to the wall behind it. Plate 7 shows an example of the jet of coolant remaining close to the wall even at very high coolant-to-free-stream pressure ratios. Fig.29 shows that, as the total pressure of the injected gas is increased, the heat transfer decreases to a fixed value at each position. It then remains at this value even if the pressure is further increased. The use of a slot thus makes it possible to inject a much greater mass flow rate into a cooling film close to the wall but there are, of course, structural limitations to the use of such slots in rotating blade arrays.

6. PREDICTION OF LIFT-OFF

Experiments at high blowing rates than that for lift-off produce results which do not show the predicted behaviour with respect to $\bar{x}$, Fig.24(a); this is hardly surprising when it is recalled that the simple theory is based on an energy balance in the boundary layer. Far downstream, however, the cooling effectiveness obtained from hole injection is very similar to that found for the slot injection case for conditions beyond lift-off. This result would indicate that a great deal of mixing has taken place between the coolant and mainstream gases and that the flow has finally become two-dimensional.

For the purposes of the design of cooling systems it would be convenient to be able to employ a single parameter which would

satisfactorily predict the onset of lift-off. It has already been seen that the momentum flux ratio $\dfrac{\rho_{si} u_i^2}{\rho_{s\infty} u_\infty^2}$ is one such parameter for the correlation of heat transfer results at fixed downstream positions; it is therefore suggested that this quantity might correlate the trajectory of the separated jets. The point of highest cooling effectiveness on the curves of $\dfrac{\rho_{si} u_i^2}{\rho_{s\infty} u_\infty^2}$ against

$\dfrac{\dot{q}_i}{\dot{q}_o}$ would obviously be just before lift-off; on inspection this was found to be at about $\dfrac{\rho_{si} u_i^2}{\rho_{s\infty} u_\infty^2} = 3.0$ for the 2 rows at 90° geometry.

The points corresponding to $\dfrac{\rho_{si} u_i^2}{\rho_{s\infty} u_\infty^2} > 3.0$ were then removed from

the plot of $\dfrac{\dot{q}_i}{\dot{q}_o}$ against $\bar{x}$; this process removed all those points which did not correlate with $\bar{x}$. The improvement can readily be seen in Fig.24(b) which has been obtained by amending Fig.24(a) in the manner described.

For the 1 row at 90° case, the same method gives a limit of $\dfrac{\rho_{si} u_i^2}{\rho_{s\infty} u_\infty^2} = 1.0$ before lift-off. Fig.25(a) is therefore amended using this limit to Fig.25(b). The improvement in correlation is not as obvious here due to the large number of points removed.

7. CONCLUSION

In this report experimental results on film cooling due to injection through rows of holes have been presented. They cover a range of Reynolds numbers and Mach numbers typical of gas turbine engine conditions. The coolant injection geometries were similar to those used in current engines and hence the results should be directly applicable to engine design; indeed, this has

been a primary aim of the work. The parameters governing film cooling in the engine situation have become more apparent, and the results have been correlated against various quantities in order to facilitate their use in engine cooling predictions, as shown in sections 4 and 5.

The results may be broadly grouped into those for double and single rows of holes. For the hole spacing-to-diameter ratios used the single rows exhibited essentially a single hole cooling characteristic as has also been shown by Eckert (9). The results for injection at both 90° and 30° showed the increase in heat transfer rate associated with "lift off" of the coolant jets as shown in Figs.9 and 10. The double rows of holes behaved in a manner between that of a single row and that of a slot, as may be seen in Figs.24 to 28. More recent research has shown that a single row of holes which expand at the surface to a "fishtail" shape also behave better than a single row of ordinary holes.

Prior to "lift-off" the single and double rows of holes produced comparable results, but as may be seen in Figs.24 to 28 this was only for low rates of coolant injection where the cooling effectiveness was in any case small. The parameter $\dfrac{\rho_{si} u_i^2}{\rho_{s\infty} u_\infty^2}$ proved to be a useful one in correlating data at a given position downstream from a given injection geometry, for a wide range of flow conditions (Figs.13 to 19). With the further restriction that only a certain flow Mach number was used, the pressure ratio $\dfrac{P_{Ti}}{P_{T\infty}}$ was found to be a useful quantity especially in that it did not involve any knowledge of hole discharge characteristics.

The slot data presented here was obtained as a check on the experimental arrangement and also to see how well the cooling

agreed with that predicted by the simple slot prediction (13).

It may be seen in Fig.28 that the agreement with this is not good.

On the other hand $\bar{x}$ does act as a fair correlating parameter for

the hole results. Analyses of the experimental results using

$\dfrac{P_{Ti}}{P_{T\infty}}$, $\dfrac{\rho_{si}u_i^2}{\rho_{s\infty}u_\infty^2}$ and $\bar{x}$ may therefore all be used for predicting

cooling, $\dfrac{P_{Ti}}{P_{T\infty}}$ being the parameter closest to the experimental

results. To date only the above elementary quantities have been

considered in detail. Further new groups which may embrace

more than one of these are under consideration and a more complex

collection of flow parameters such as that in Brown (13) may

finally be chosen as more suitable. Another approach which is

to be undertaken is to compare the prediction of numerical proce-

dures such as that of Patankar and Spalding (14) with the experi-

mental results.

The authors hope that the results presented here will serve

the purpose of providing data immediately relevant to turbine

design. They should also provide a test for any new predictive

techniques for the three-dimensional problem of film cooling with

injection through holes.

8. <u>NOMENCLATURE</u>

a_h - area of an injection hole

a (other suffices) - velocity of sound

A_N - area of working section of nozzle

A^* - area of throat of nozzle

$\left.\begin{array}{l}A) \\ B)\end{array}\right.$ - constants in simple film cooling theory

C_D - discharge coefficient

d   - diameter of an injection-hole

h   - heat transfer coefficient

I   - mass flux ratio $\dfrac{\rho_{si} u_i}{\rho_{s\infty} u_\infty}$

J   - momentum flux ratio $\dfrac{\rho_{si} u_i^2}{\rho_{s\infty} u_\infty^2}$

K   - energy flux ratio $\dfrac{\rho_{si} u_i^3}{\rho_{s\infty} u_\infty^3}$

$\dot{m}$ - mass flow rate

M   - Mach number

N   - number of injection holes

P   - pressure

$\dot{q}$ - heat transfer rate

r   - spacing of rows of injection holes (see Fig.2(c))

R   - gas constant per unit mass

Re   - Reynolds' number

s   - spanwise spacing of injection holes

S   - slot height

t   - time

T   - temperature

u   - velocity

V   - volume

x	- distance downstream from injection holes
$\bar{x}$	- parameter used in simple film cooling theory
y	- distance from centreline in spanwise direction
γ	- ratio of specific heats
η	- film cooling effectiveness
μ	- viscosity
ρ	- density

Suffices

aw	- adiabatic wall
i	- injection
o	- without injection
s	- static
T	- total
∞	- free stream

References

| No. | Title, Author(s), etc. |

1   Hot-air discharge for de-icing.- K. Wieghardt. AAF Translation, Report No. F-Ts-919-Re, Wright Field, Ohio. 1946.

2   An experimental investigation of turbulent slot injection at Mach 6.- K. Parthasarathy and V. Zakkay. AIAA Journal, Vol.8, No.7, p.1302. 1969.

3   Olympus 593 turbine cooling.- M.J. Holland. AGARD Conference Proceedings No.73. High Temperature Turbines. 1971.

4   Film cooling.- R.J. Goldstein. Advances in Heat Transfer, Vol.7, Ed. T.F. Irvine and J.P. Hartnett, (Academic Press). 1971.

5   A study of film cooling related to gas turbines using transient techniques.- T.V. Jones and D.L. Schultz. A.R.C.32 420. 1970.

6   Film cooling studies in subsonic and supersonic flows using a shock tunnel.- T.V. Jones and D.L. Schultz. Shock Tube Research, Proc. 8th Int. Shock Tube Symp., Ed. J.L. Stollery, A.G. Gaydon and P.R. Owen, (Chapman and Hall). 1971.

7   The results of the feasibility study conducted under agreement B/SR/8986.- T.V. Jones and D.L. Schultz. Oxford University Engineering Laboratory Report No.1009/71. 1971.

8   Heat-transfer measurements in short duration hypersonic facilities.- D.L. Schultz and T.V. Jones. AGARDograph No.165, AGARD-NATO. 1973.

9   Film cooling with injection through holes.- E.R.G. Eckert. AGARD Conference Proceedings No.73. High Temperature Turbines. 1971.

10 Film cooling following injection through inclined circular tubes.- R.J. Goldstein, E.R.G. Eckert, V.L. Eriksen and J.W. Ramsey. Israel Journal of Technology, Vol.8, No.1-2, pp.145-154. 1970.

11 Application of film cooling to gas-turbine blades.- C. Liess and J. Carnel. AGARD Conference Proceedings, No.73, High Temperature Turbines. 1971.

12 A note on the use of a boundary layer model for correlating film-cooling data.- J.L. Stollery and A.A.M. El-Ehwany. Int.J. Heat Mass Transfer, Vol.8, pp.55-65. 1965.

13 A theoretical and experimental investigation into film cooling.- A. Brown. Japan Society of Mechanical Engineers Semi-International Symposium. 1967.

14 Heat and mass transfer in boundary layers.- S.V. Patankar and D.B. Spalding. 2nd edition (Intertext). 1970.

KEY TO SYMBOLS USED IN GRAPHS

$T_{T\infty}$,°K / $P_{T\infty}$ p.s.i.a.	1000 / 330	500 / 480	1000 / 240	500 / 370	2000 / 290	2000 / 90
$M_\infty = 0.2$	△	▲			⟁	⚠
0.5	♂	◖	○	●		
0.7	+	×				
1.86			◇	◆		

Figure 26.   Graph of $\frac{\dot{q}_i}{\dot{q}_o}$ against $\bar{x}$.   2 rows at 30°.

IRON SLUG ┌DIAPHRAGM BURSTING PIN

COIL┐

DIAPHRAGMS⟍   INJECTION GAS

                    NOZZLE LINERS

                    VALVE   SONIC THROAT

SHOCK   SCHLIEREN   DUMP
TUBE   WINDOW   TANK

                                    STATIC PRESSURE
INJECTION   TAPPINGS
HOLES

POSITIONS OF
HEAT TRANSFER
GAUGES

(a) WORKING SECTION

y(mm)   0   10   20   30   40   x(mm)
10
5
0   II   II   I   I   I

THIS ROW
BLOCKED   INJECTION
FOR 1 ROW HOLES   HEAT TRANSFER GAUGES
CASE

(b) FLOOR PLAN SHOWING POSITIONS OF HEAT TRANSFER
GAUGES.

d=0·5mm $^s/d=2·5$ $^l/d=5$ $\theta=90°$ OR $30°$

$\frac{r}{s}=\frac{\sqrt{3}}{2}$ $(\frac{\sqrt{3}}{4}$ IN ONE CASE : SEE TEXT)

NUMBER OF ROWS n = 1 OR 2
NUMBER OF HOLES N = 12 OR 25

(c) KEY TO HOLE CONFIGURATIONS.

Figure 2.   Details of the working section.
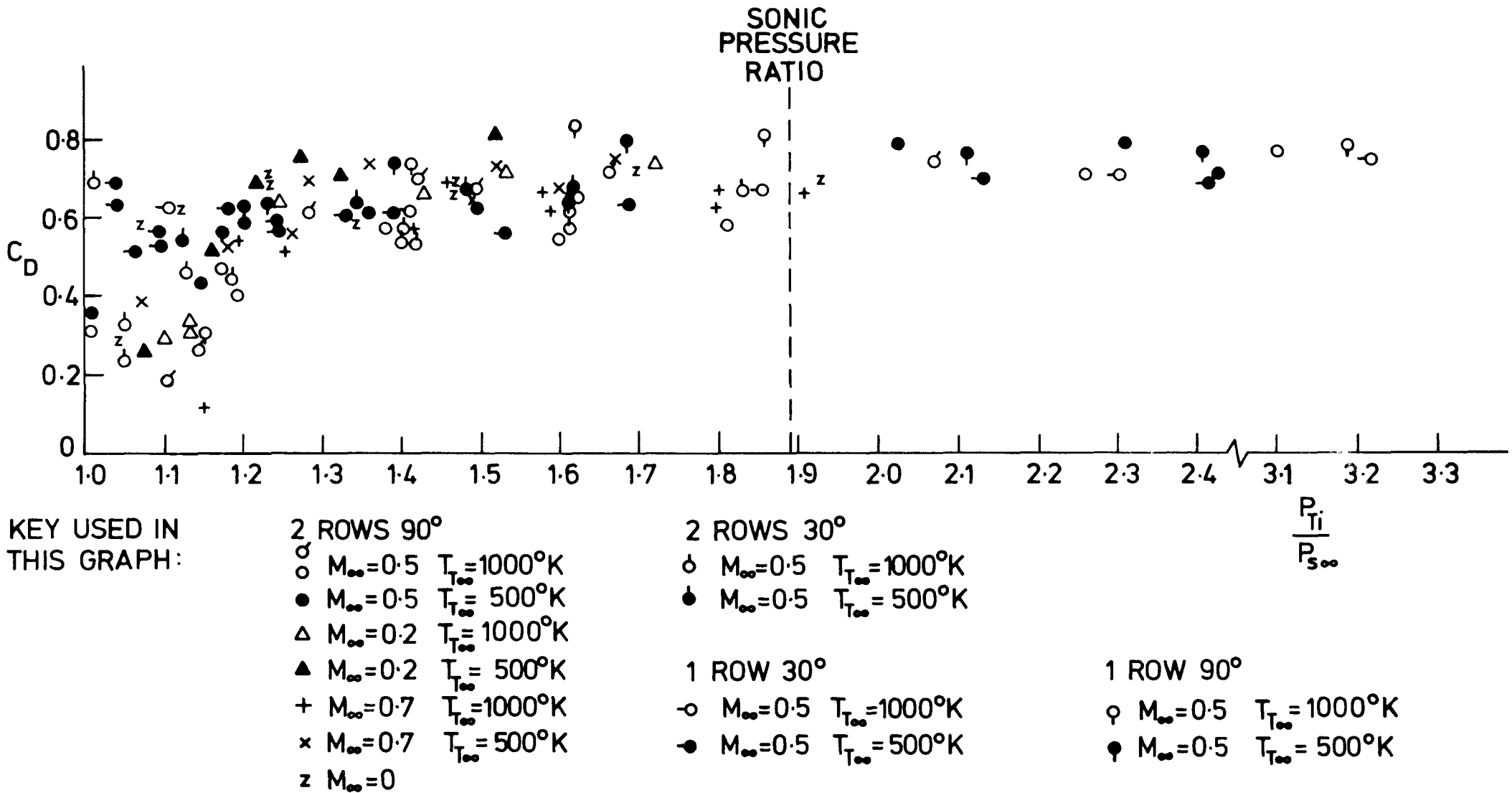
Figure 3.   Graph of discharge coefficient C_D against $\dfrac{P_{Ti}}{P_{s\infty}}$.   All hole geometries and Mach numbers.
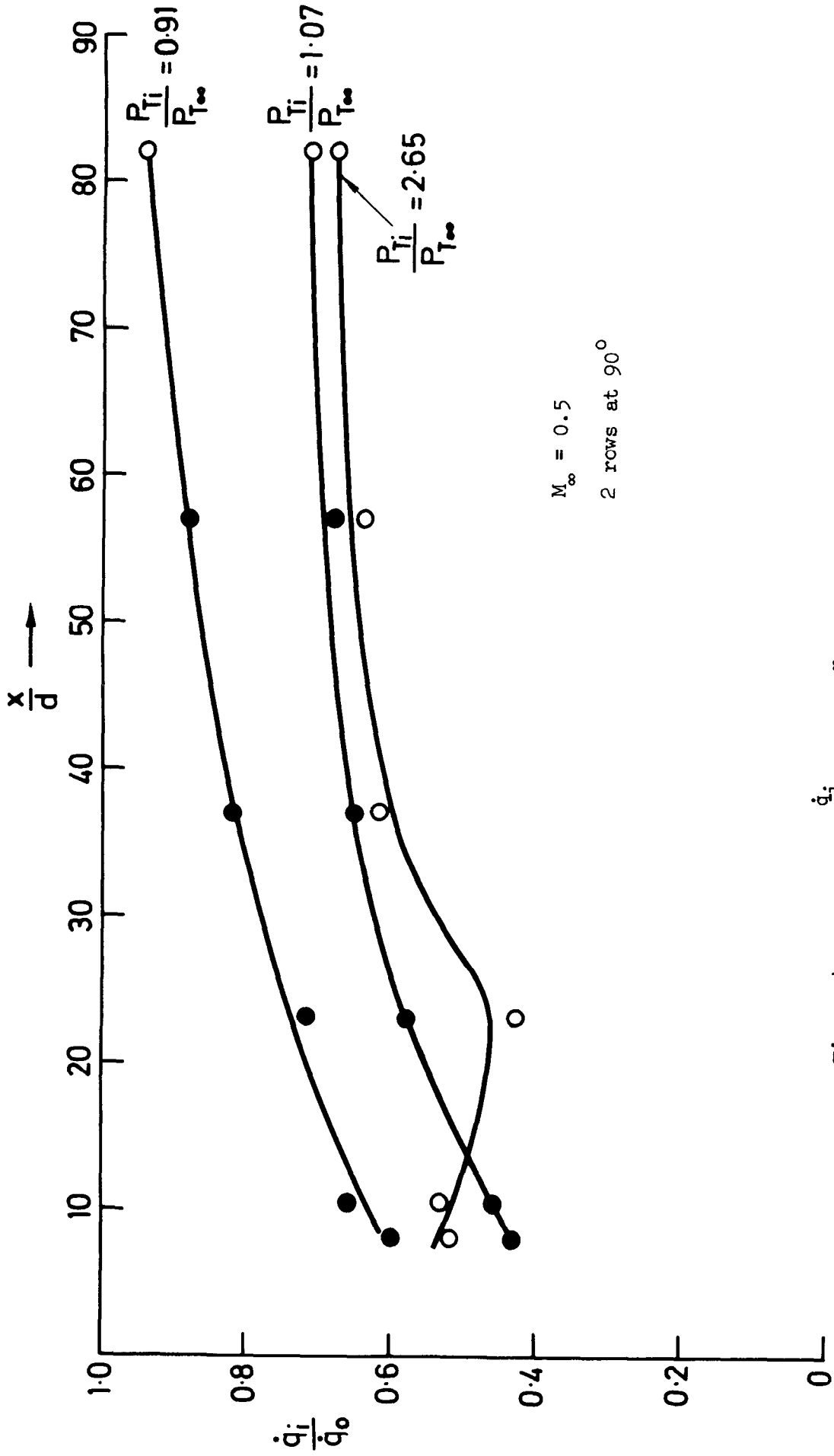
Figure 4. Graph of $\dfrac{\dot{q}_i}{\dot{q}_o}$ against $\dfrac{x}{d}$ for three pressure ratios.
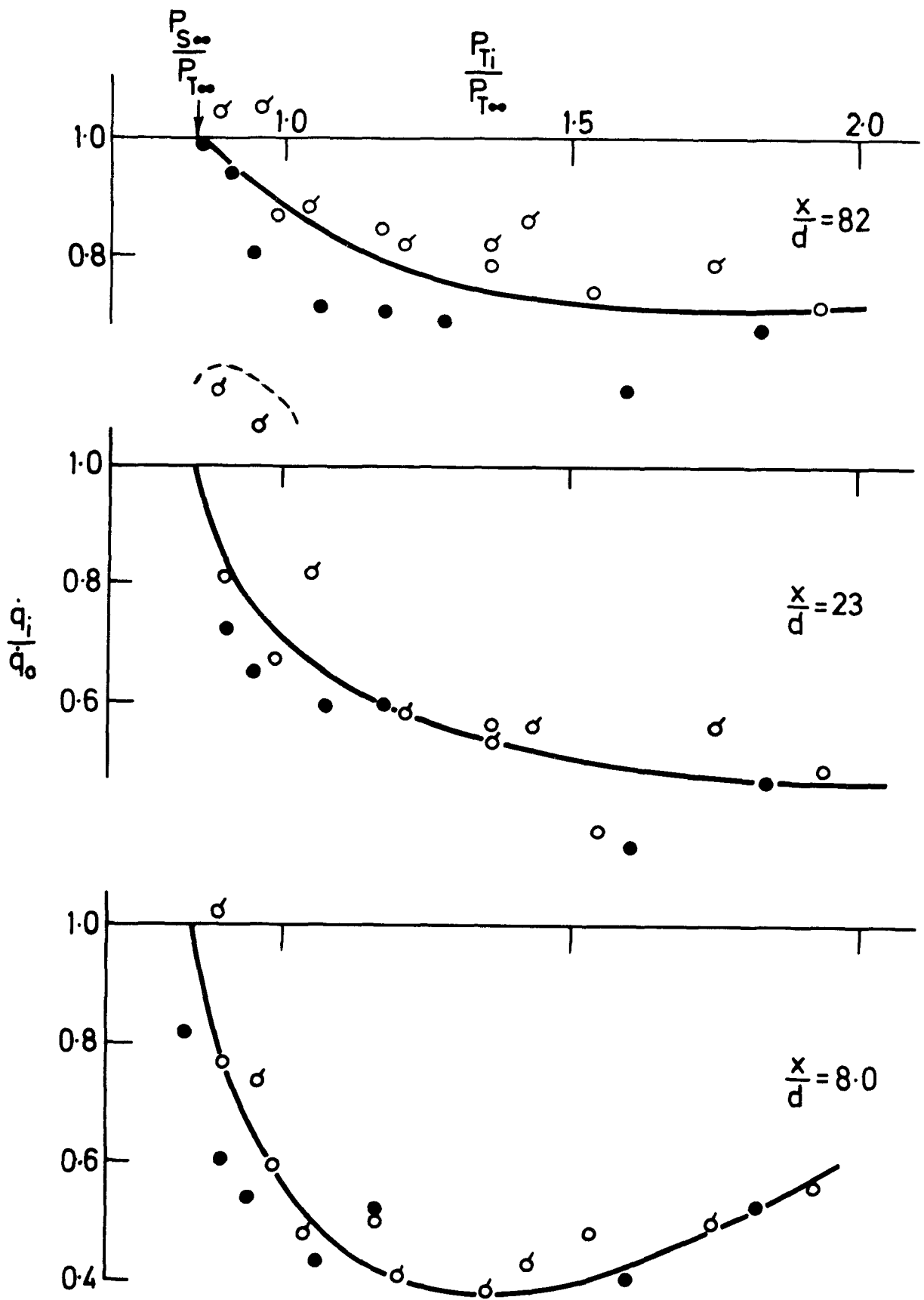
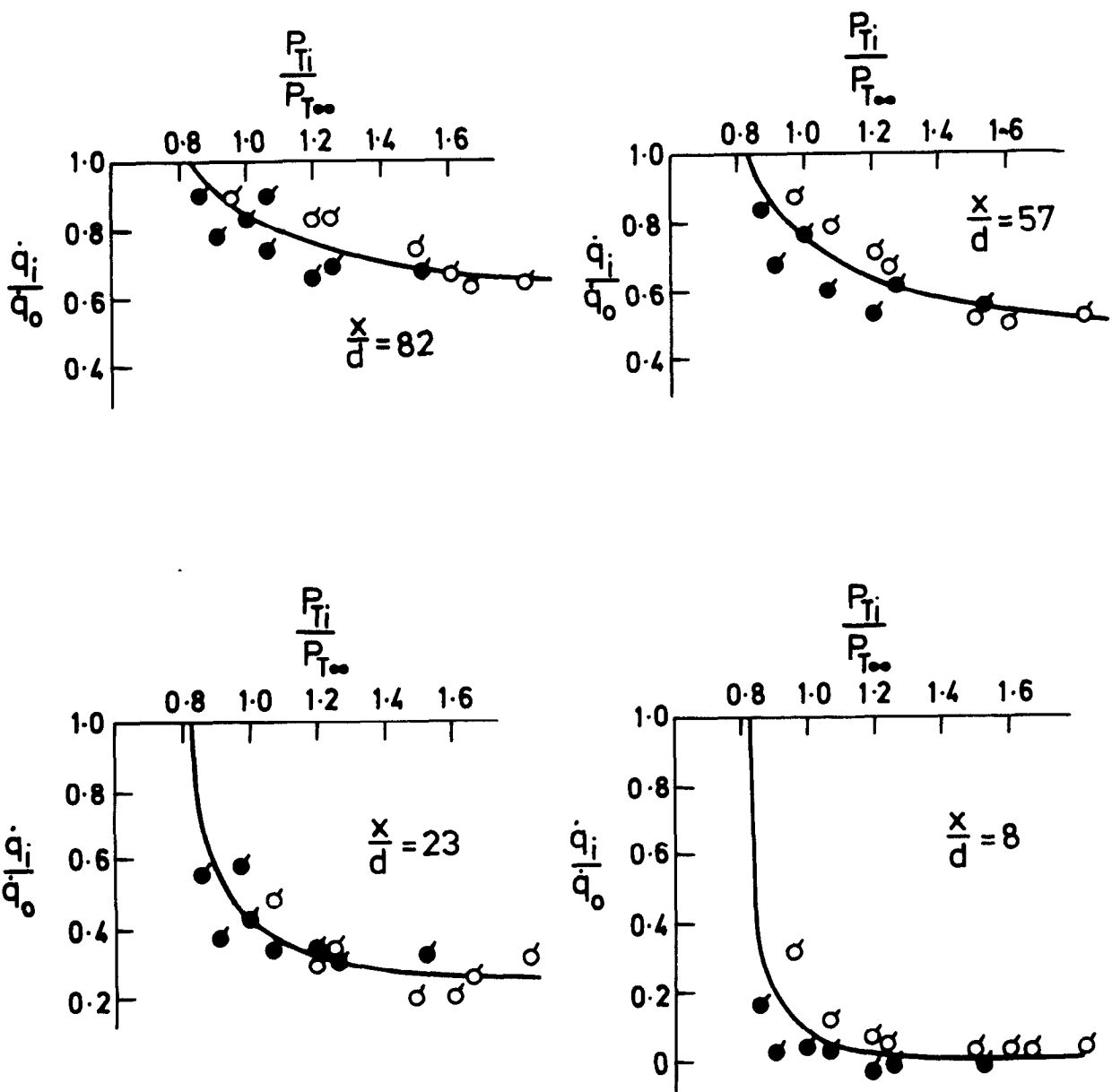Figure 5.   Graphs of $\frac{\dot{q}_i}{\dot{q}_o}$ against $\frac{P_{Ti}}{P_{T\infty}}$. $M_\infty = 0.5$, 2 rows at 90°.
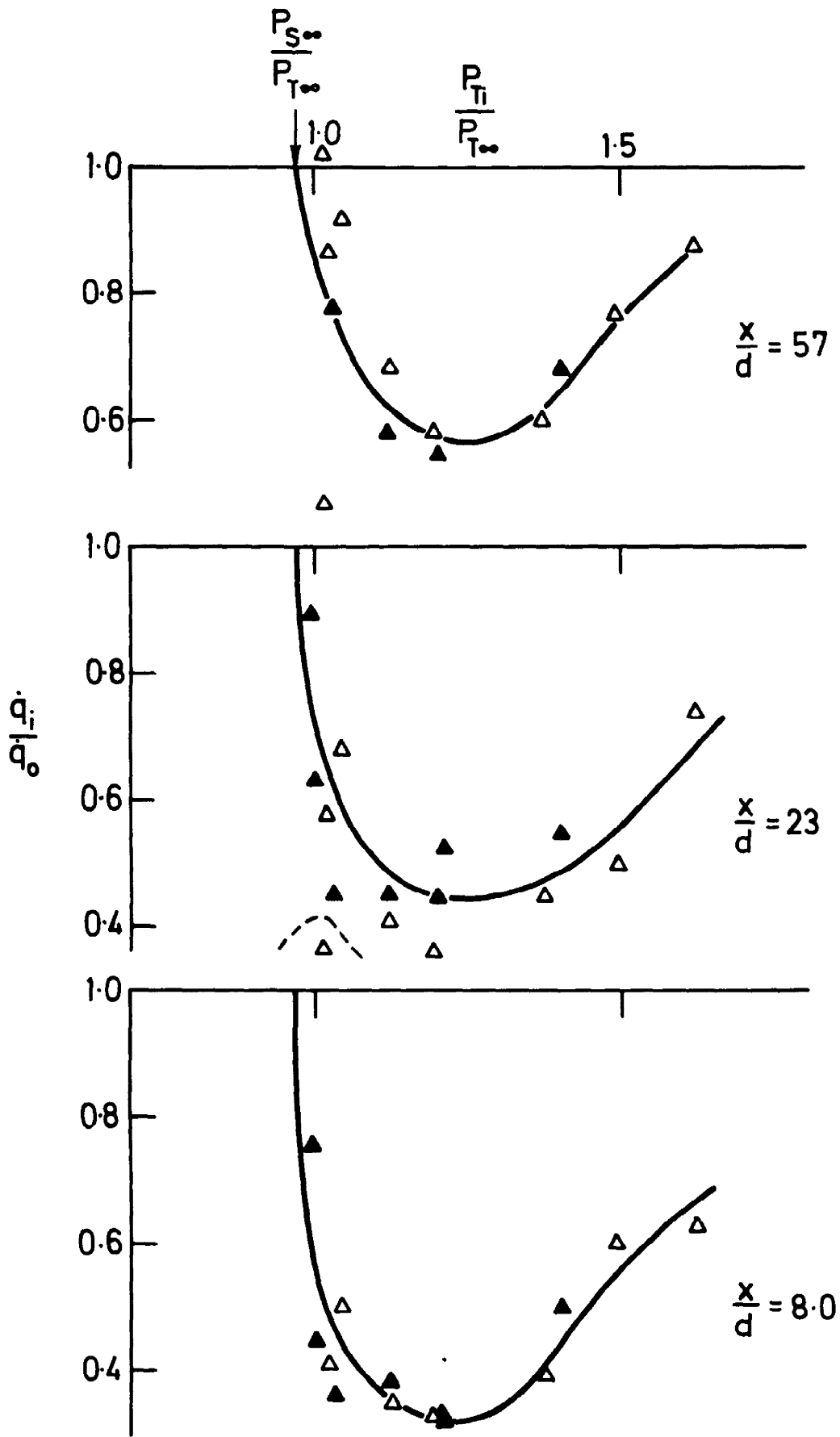
Figure 6. Graphs of $\dfrac{\dot{q}_i}{\dot{q}_o}$ against $\dfrac{P_{Ti}}{P_{T\infty}}$. $M_\infty = 0.2$, 2 rows at 90°.
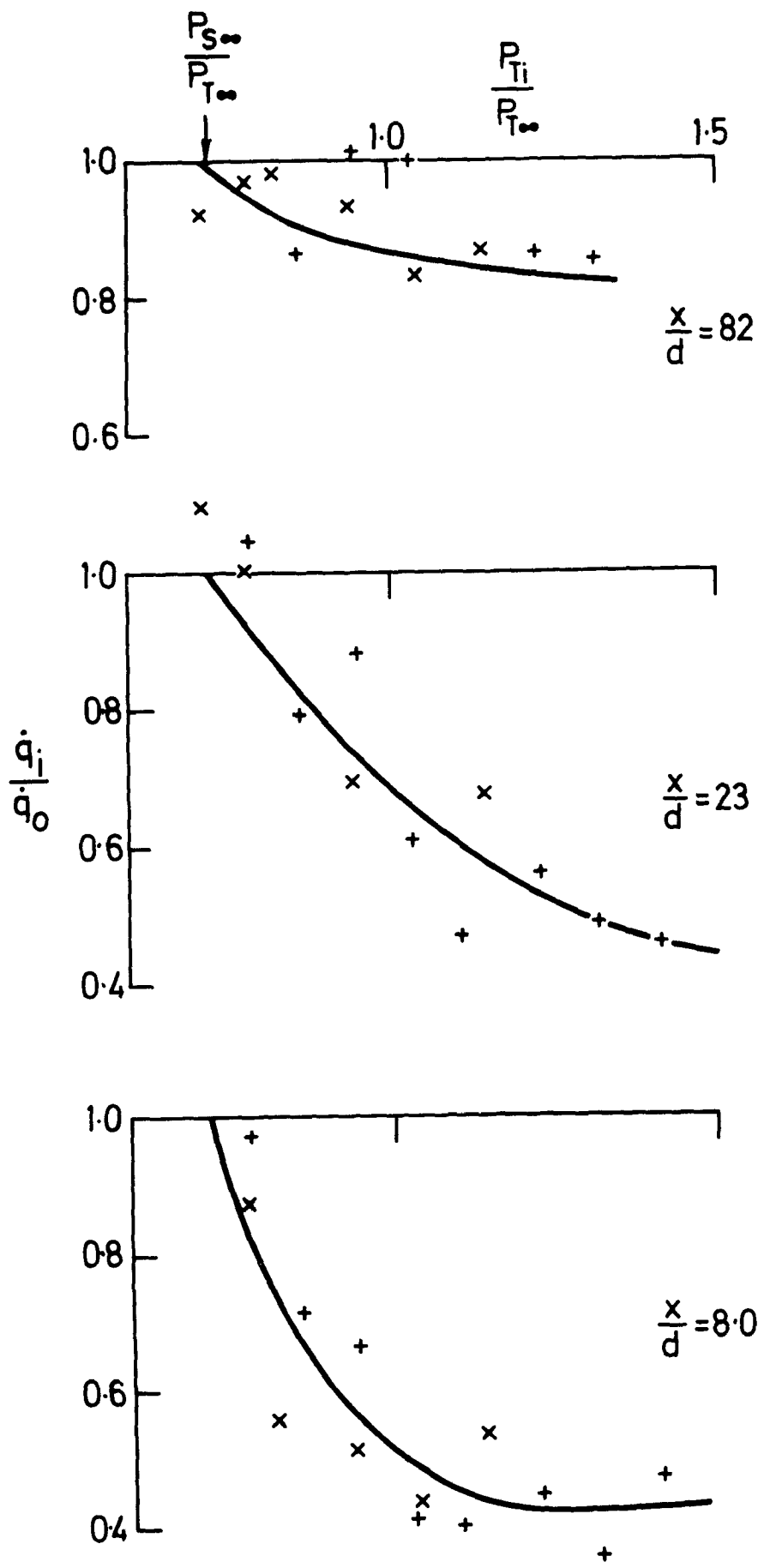
Figure 7. Graphs of $\frac{\dot{q}_i}{\dot{q}_o}$ against $\frac{P_{Ti}}{P_{T\infty}}$. $M_\infty = 0.7$, 2 rows at $90°$.
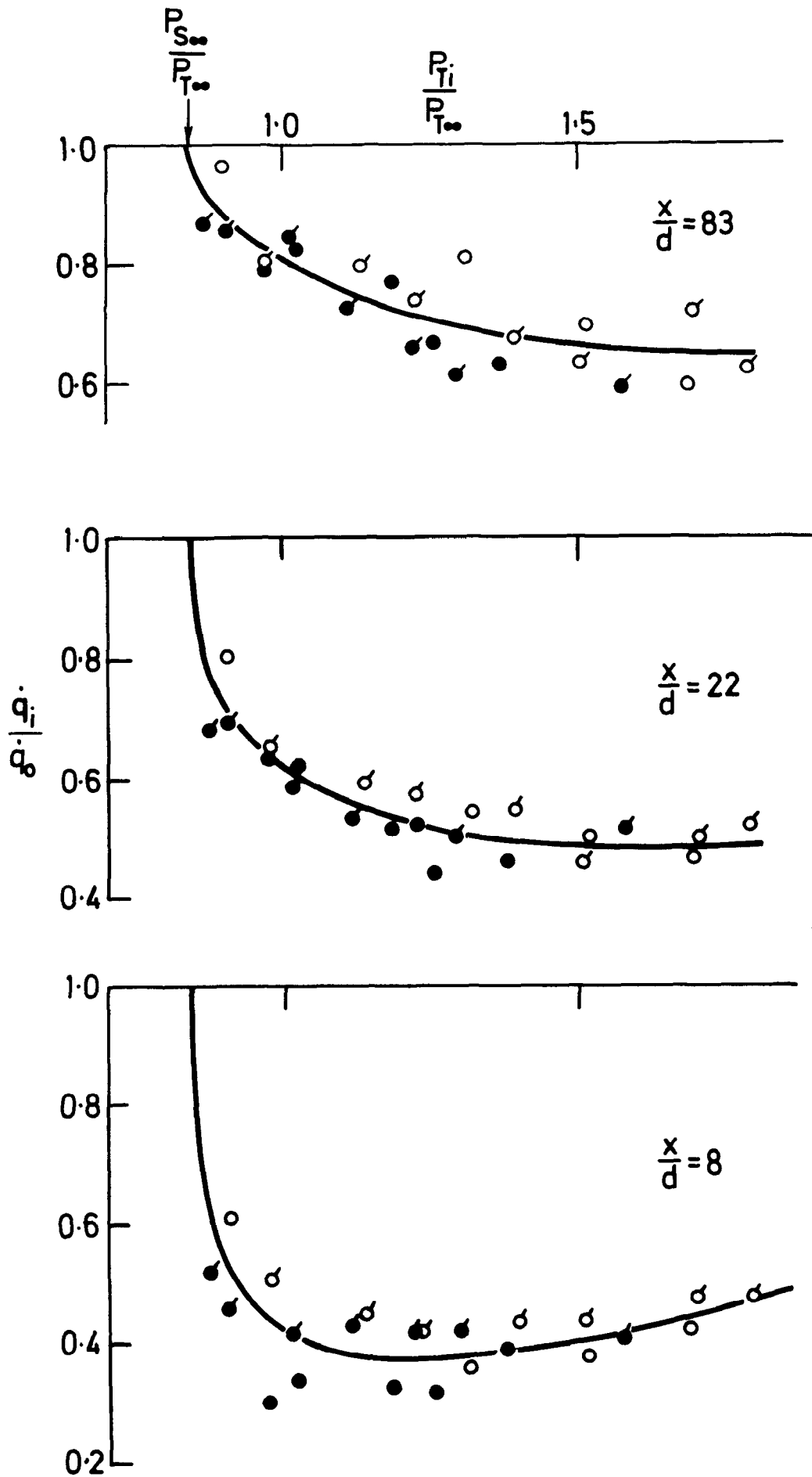
Figure 8.   Graphs of $\dfrac{\dot{q}_i}{\dot{q}_o}$ against $\dfrac{P_{Ti}}{P_{T\infty}}$. $M_\infty = 0.5$, 2 rows at $30°$.
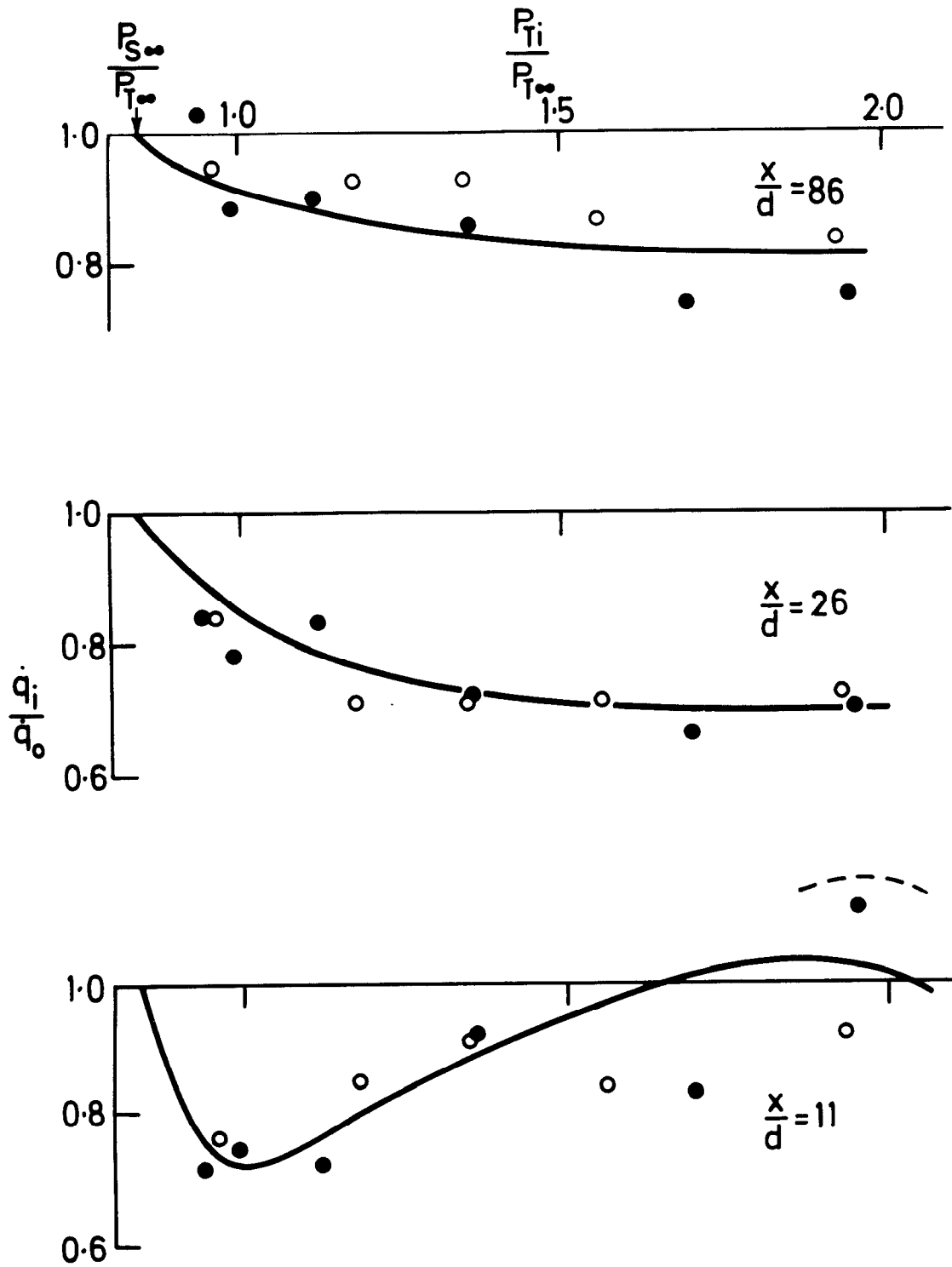
Figure 9. Graphs of $\frac{\dot{q}_i}{\dot{q}_o}$ against $\frac{P_{Ti}}{P_{T\infty}}$. $M_\infty = 0.5$, 1 row at 90°.
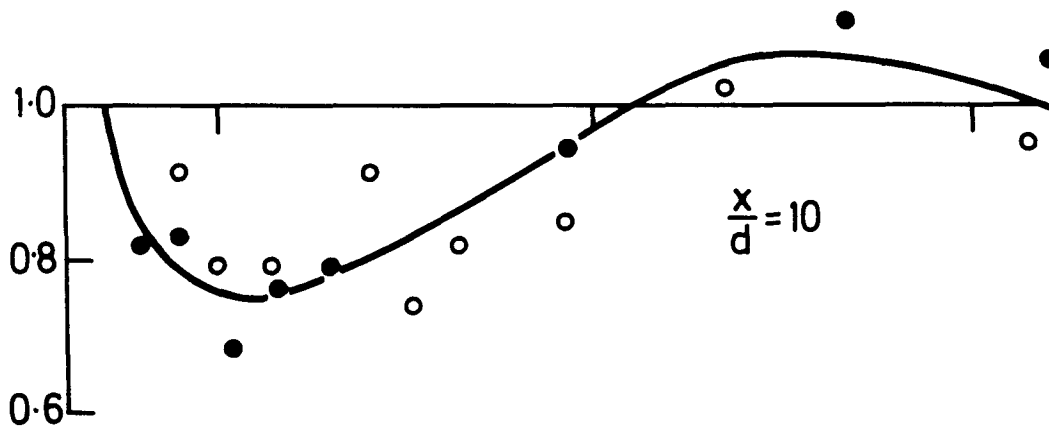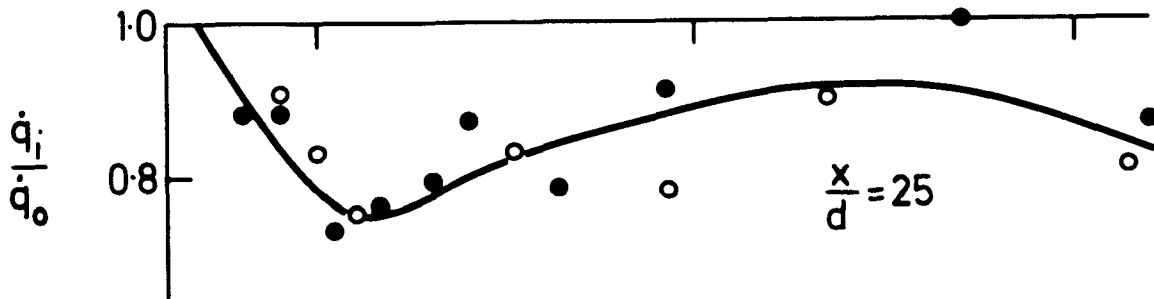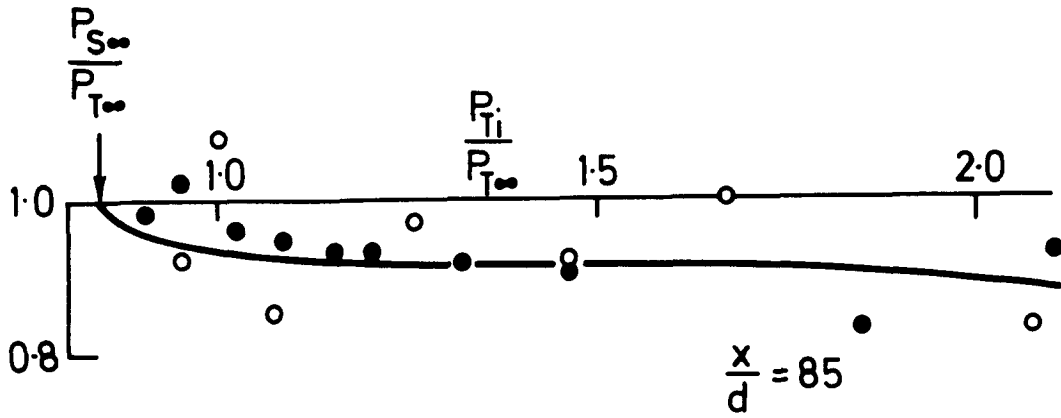
Figure 10. Graphs of $\dfrac{\dot{q}_i}{\dot{q}_o}$ against $\dfrac{P_{Ti}}{P_{T\infty}}$. $M_\infty = 0.5$, 1 row at 30°.
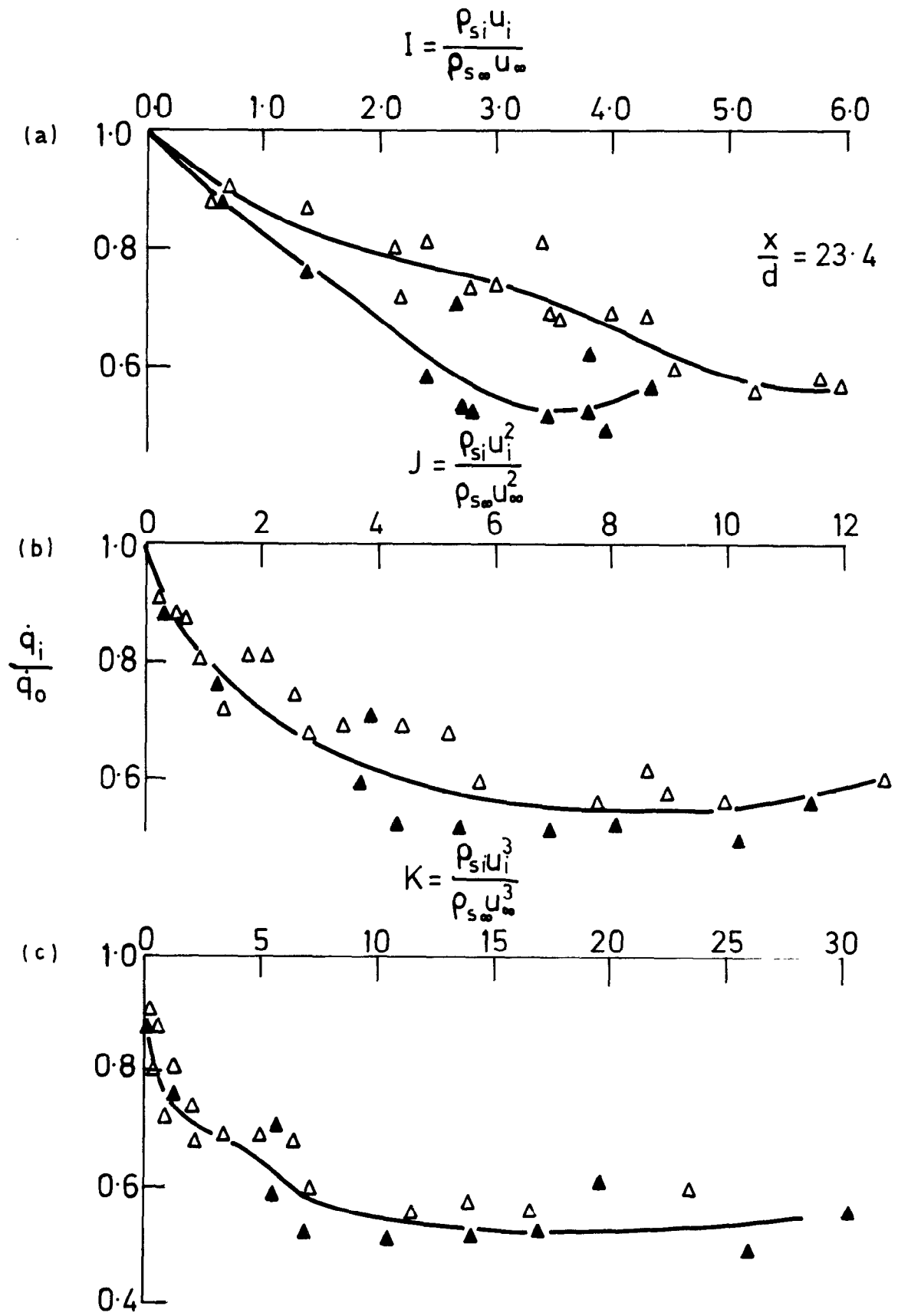
Figure 11 (a), (b) and (c). Graphs of $\dfrac{\dot{q}_i}{\dot{q}_o}$ against I, J and K respectively. $M_\infty = 0.2$, 1 row at $90°$, $\dfrac{x}{d} = 23$.
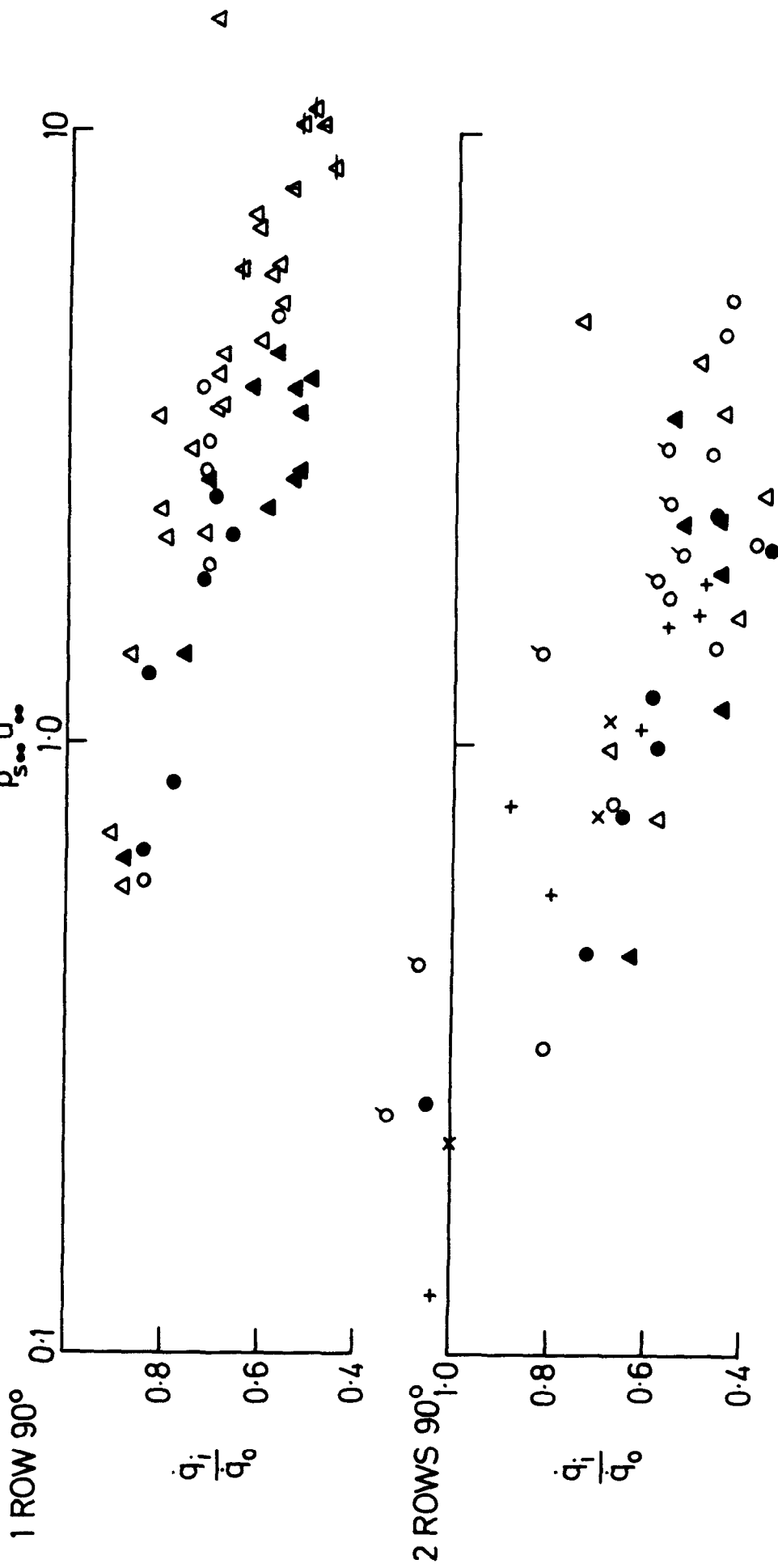
Figure 12(a). Graphs of $\frac{\dot{q}_i}{\dot{q}_o}$ against $I = \frac{\rho_{si} u_i}{\rho_{s\infty} u_\infty}$. $\frac{x}{d} = 23$.
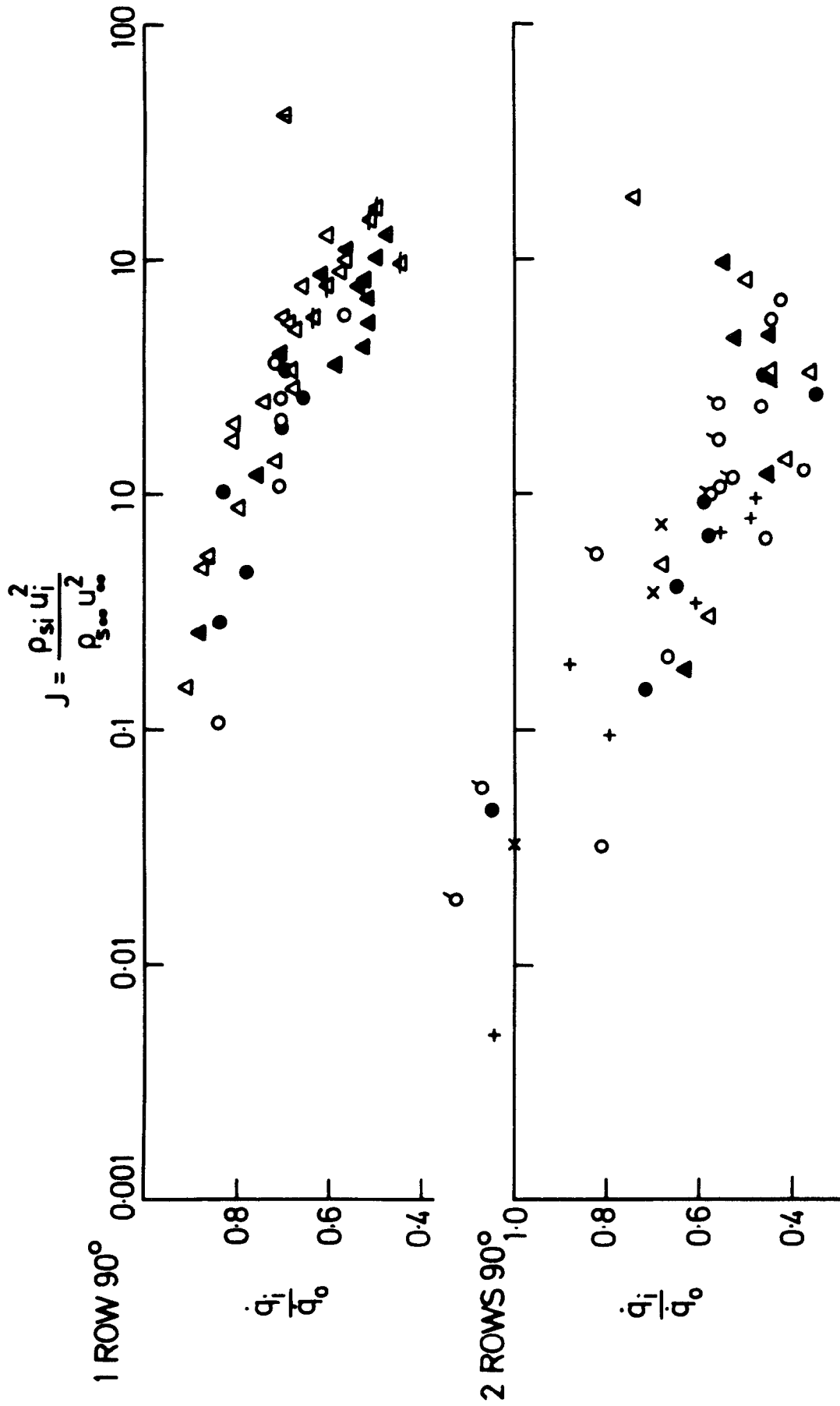
Figure 12(b). Graphs of $\dfrac{\dot{q}_i}{\dot{q}_o}$ against $J = \dfrac{\rho_{si} u_i^{\ 2}}{\rho_{s\infty} u_\infty^{\ 2}}$. $\dfrac{x}{d} = 23$.
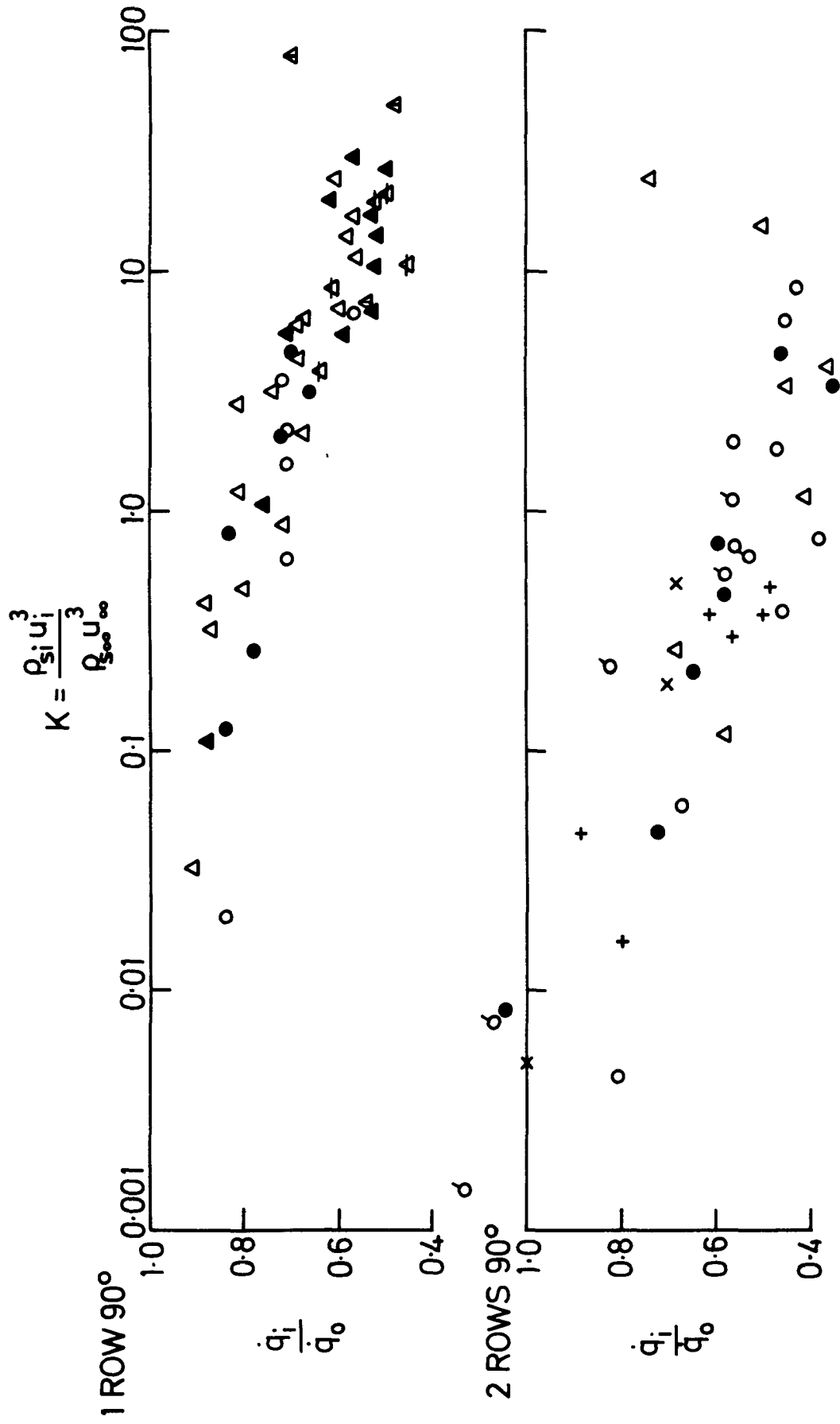
Figure 12(c). Graphs of $\dfrac{\dot{q}_i}{\dot{q}_o}$ against $K = \dfrac{\rho_{si} u_i^3}{\rho_{s\infty} u_\infty^3}$. $\dfrac{x}{d} = 23$.
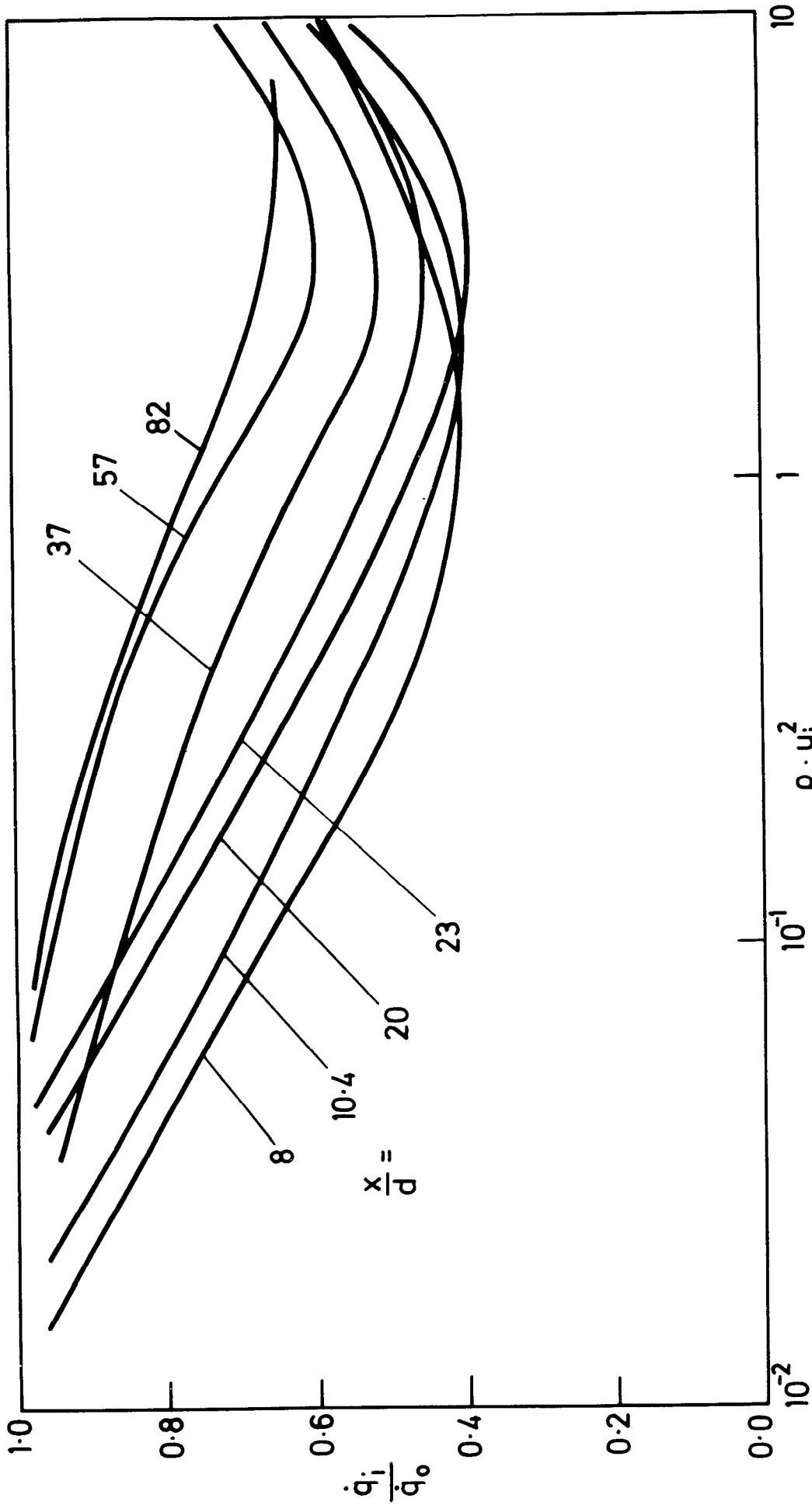
Figure 13. Mean lines of data plotted as $\dfrac{\dot{q}_i}{\dot{q}_o}$ against $\dfrac{\rho_{si}u_i^2}{\rho_{s\infty}u_\infty^2}$. 2 rows at $90°$.
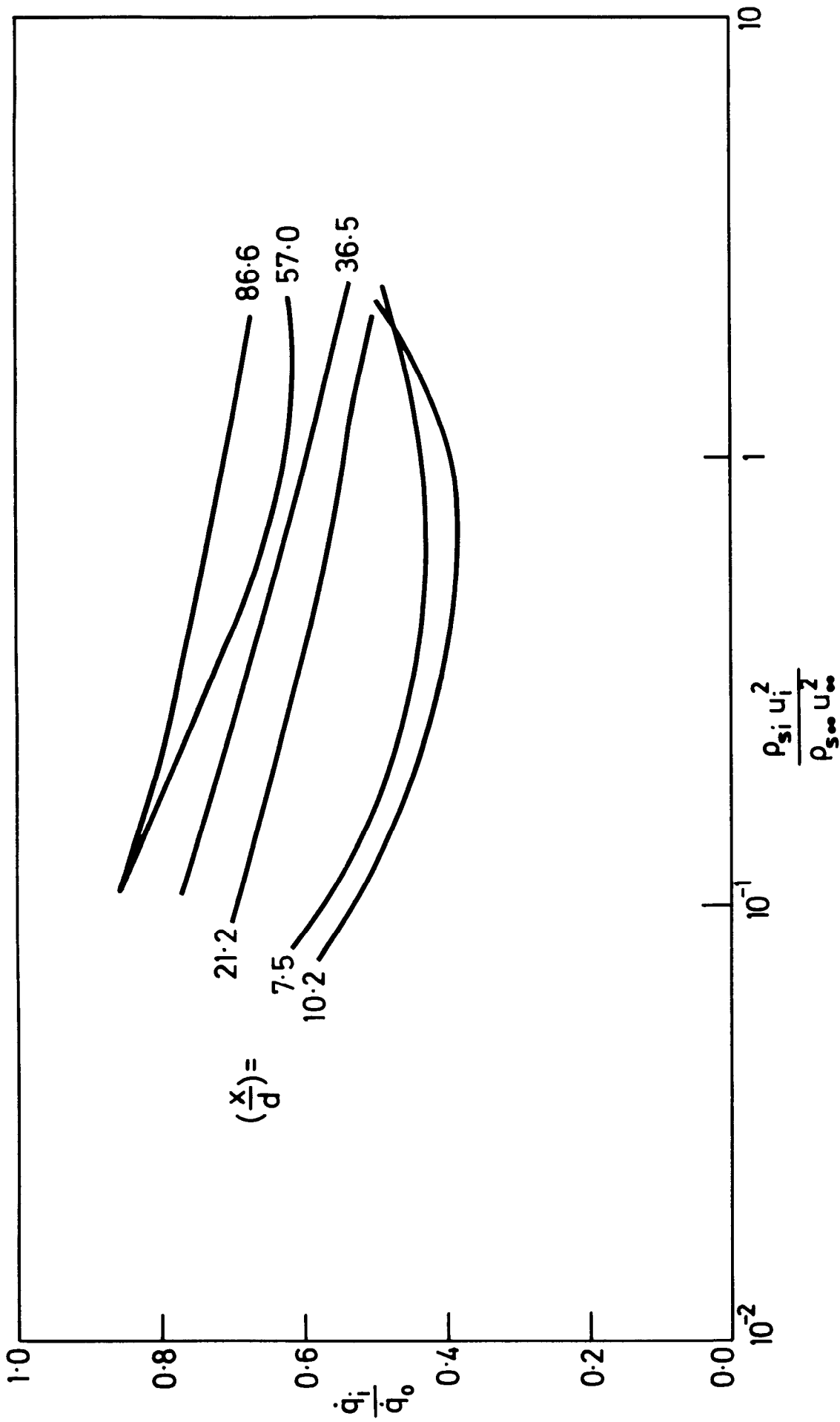
Figure 14. Mean lines of data plotted as $\frac{\dot{q}_i}{\dot{q}_o}$ against $\frac{\rho_{si} u_i^2}{\rho_{s\infty} u_\infty^2}$. 2 rows at 30°. $(\frac{r}{s} = \frac{\sqrt{3}}{2})$.
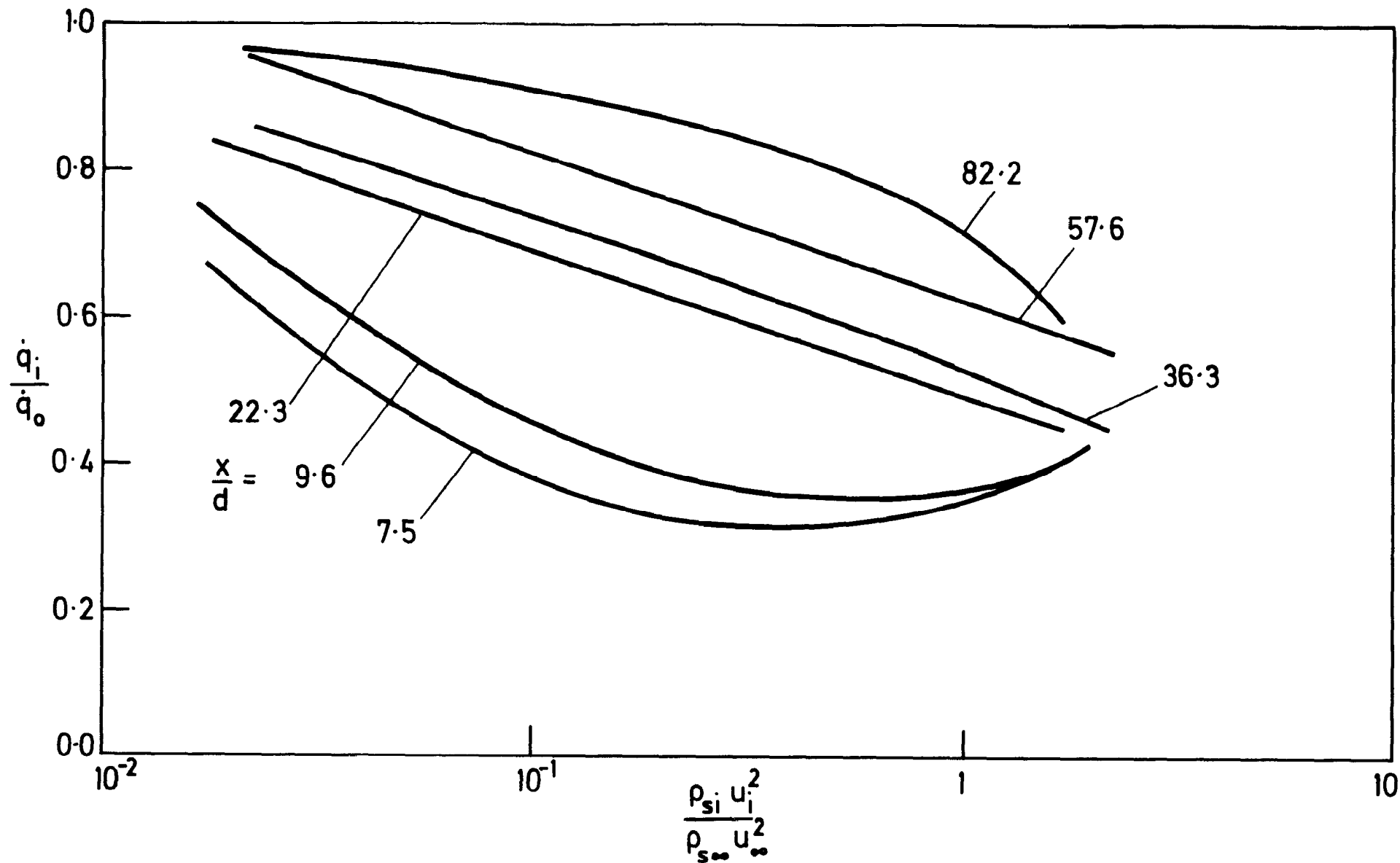
Figure 15. Mean lines of data plotted as $\dfrac{\dot{q}_i}{\dot{q}_o}$ against $\dfrac{\rho_{si} u_i^2}{\rho_{s\infty} u_\infty^2}$. 2 rows at 30°. $(\dfrac{r}{s} = \dfrac{\sqrt{3}}{4})$.
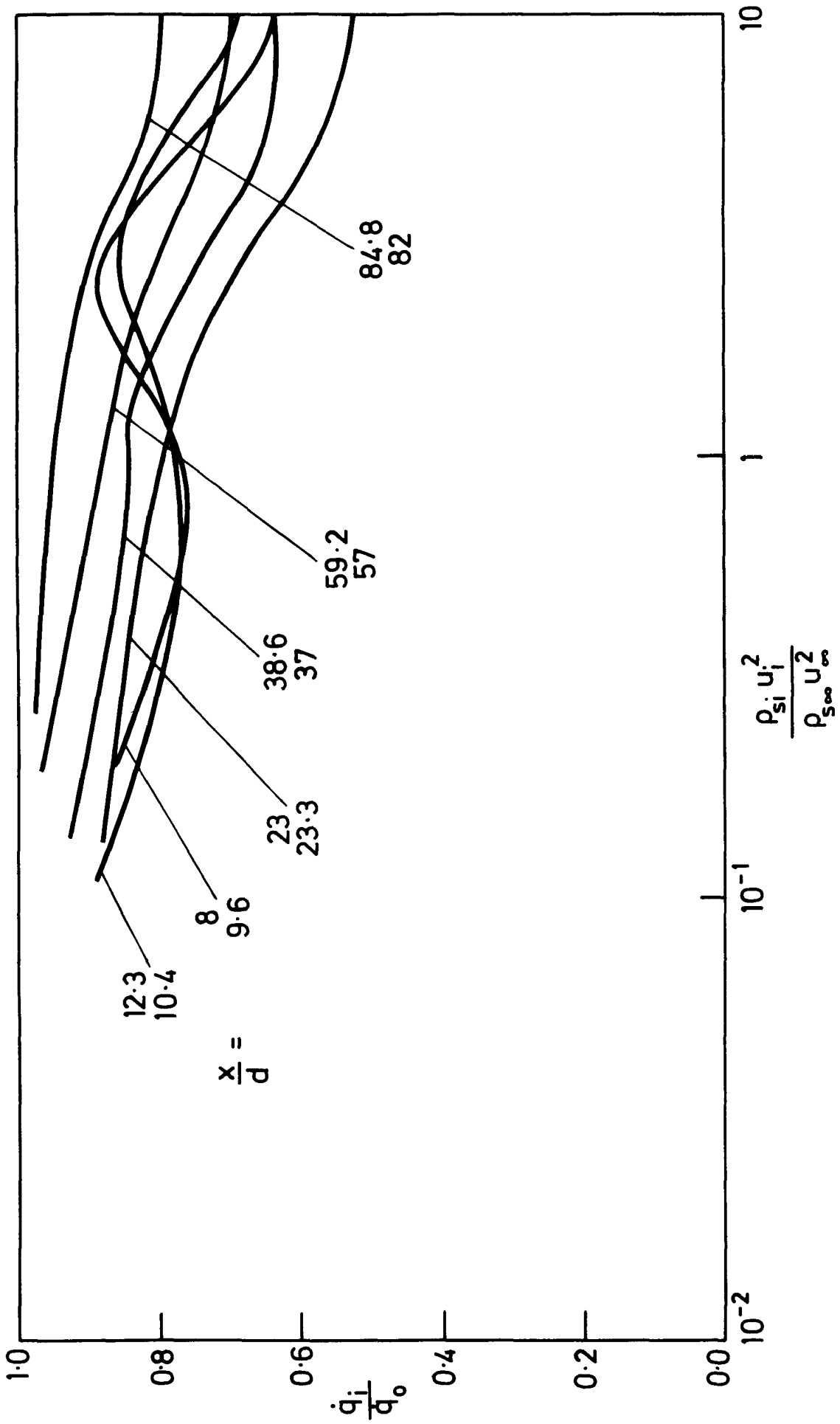
Figure 16. Mean lines of data plotted as $\dfrac{\dot{q}_i}{\dot{q}_o}$ against $\dfrac{\rho_{si} u_i^2}{\rho_{s\infty} u_\infty^2}$. 1 row at $90°$.
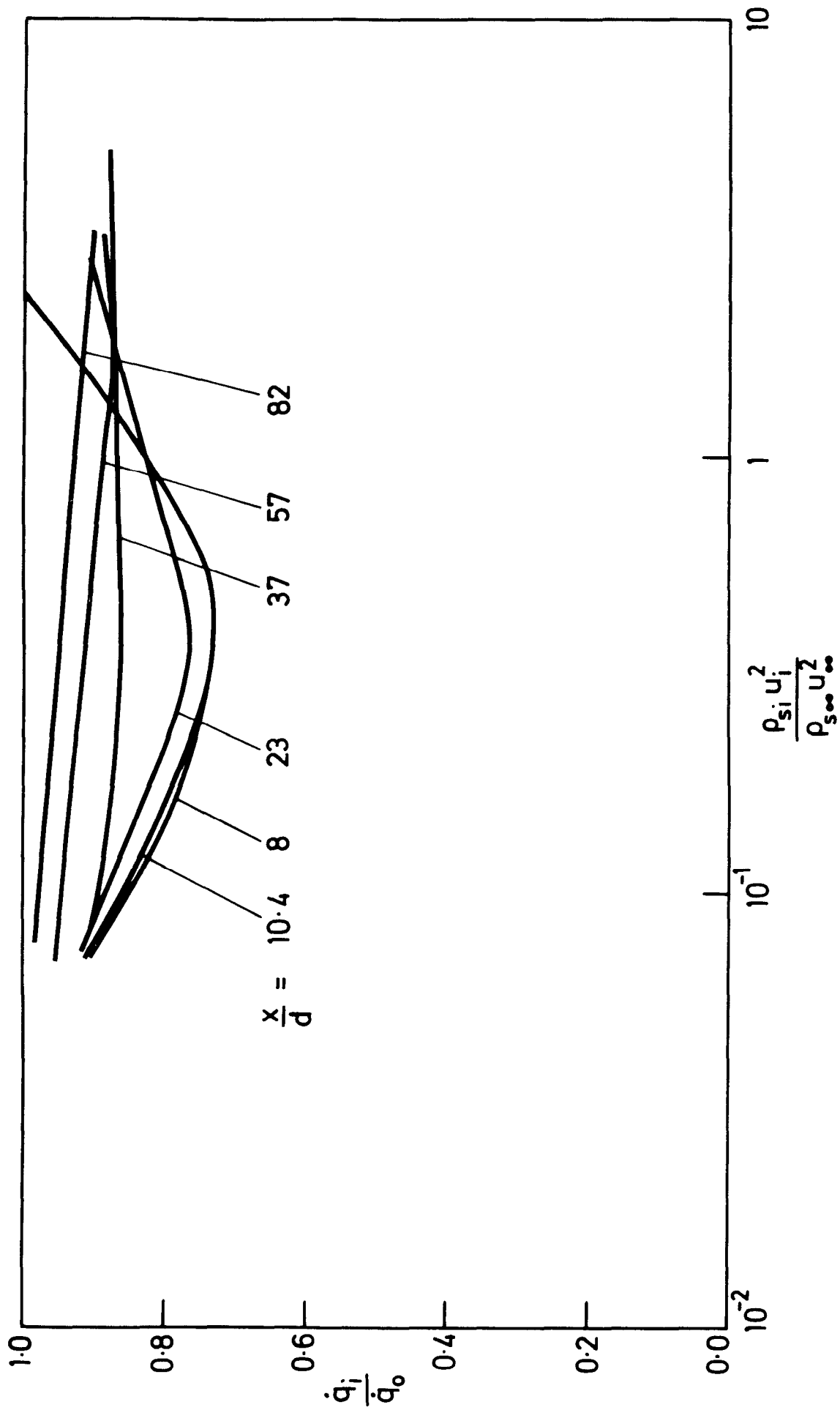
Figure 17. Mean lines of data plotted as $\dfrac{\dot{q}_i}{\dot{q}_o}$ against $\dfrac{\rho_{si} u_i^2}{\rho_{s\infty} u_\infty^2}$. 1 row at 30°.
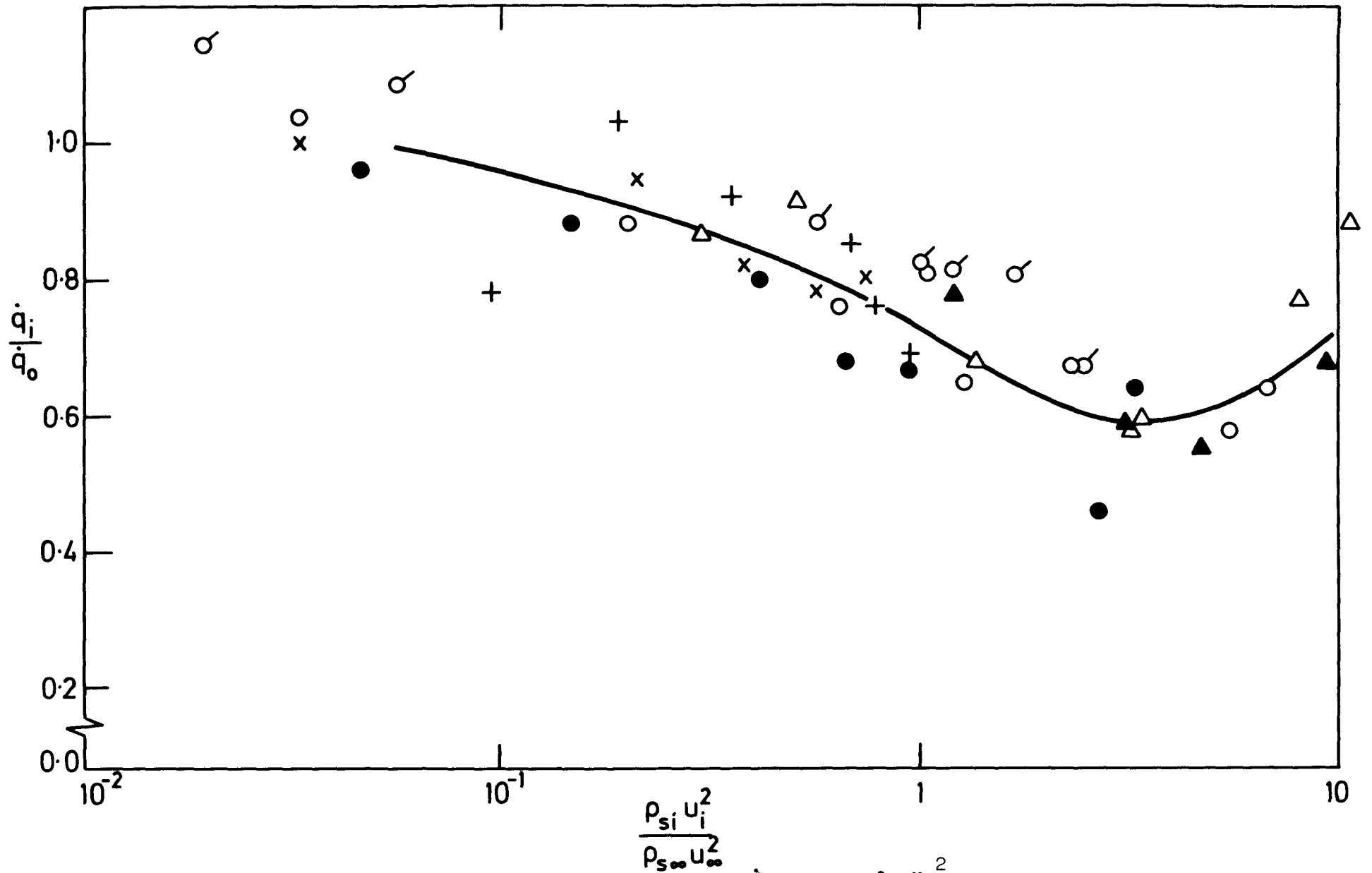
Figure 18. Typical scatter of data about mean line $\dfrac{\dot{q}_i}{\dot{q}_o}$ against $\dfrac{\rho_{si} u_i^2}{\rho_{s\infty} u_\infty^2}$. 2 rows at $90°$. $\dfrac{x}{d} = 57$.
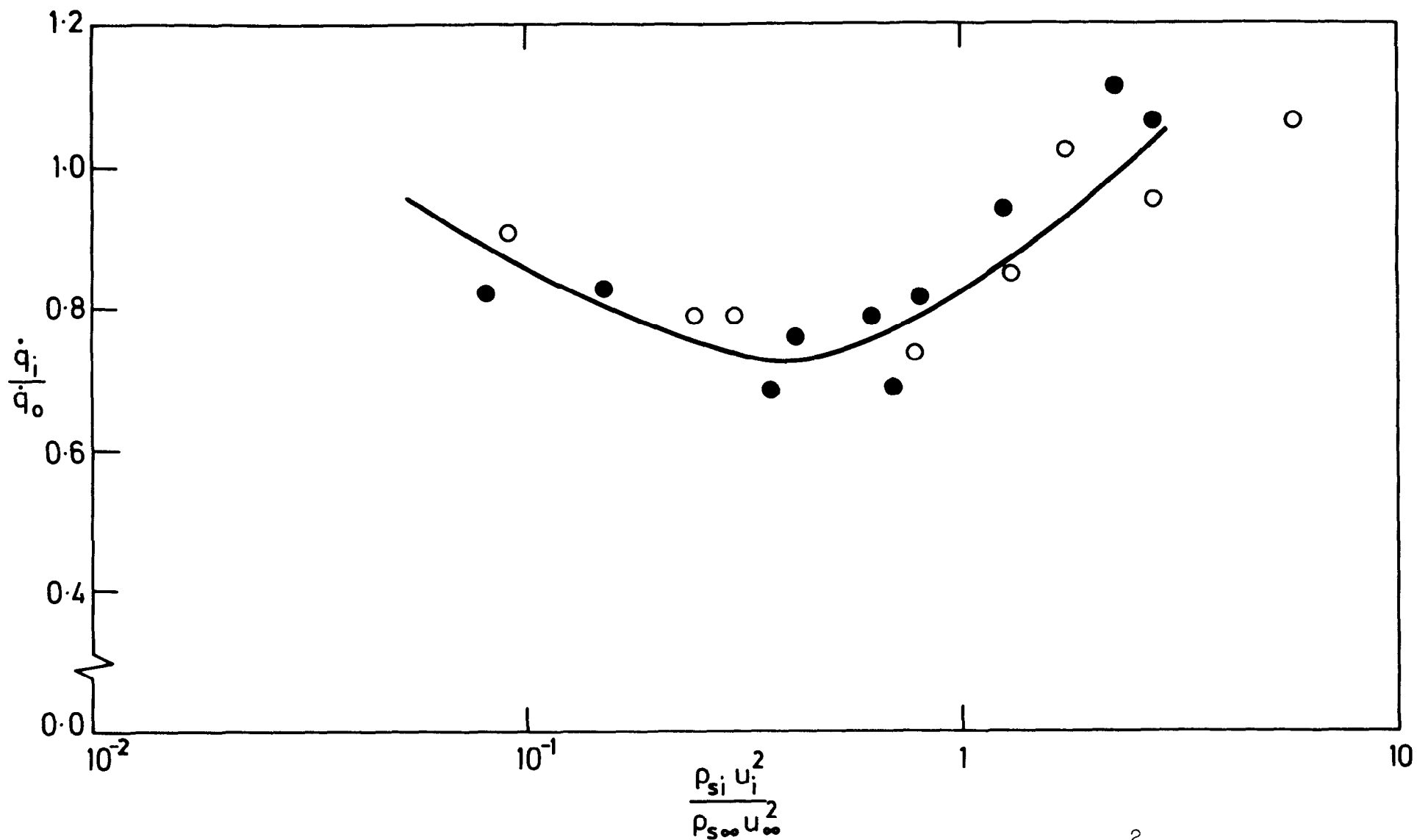
Figure 19. Typical scatter of data about mean line. $\frac{\dot{q}_i}{\dot{q}_o}$ against $\frac{\rho_{si} u_i^2}{\rho_{s\infty} u_\infty^2}$
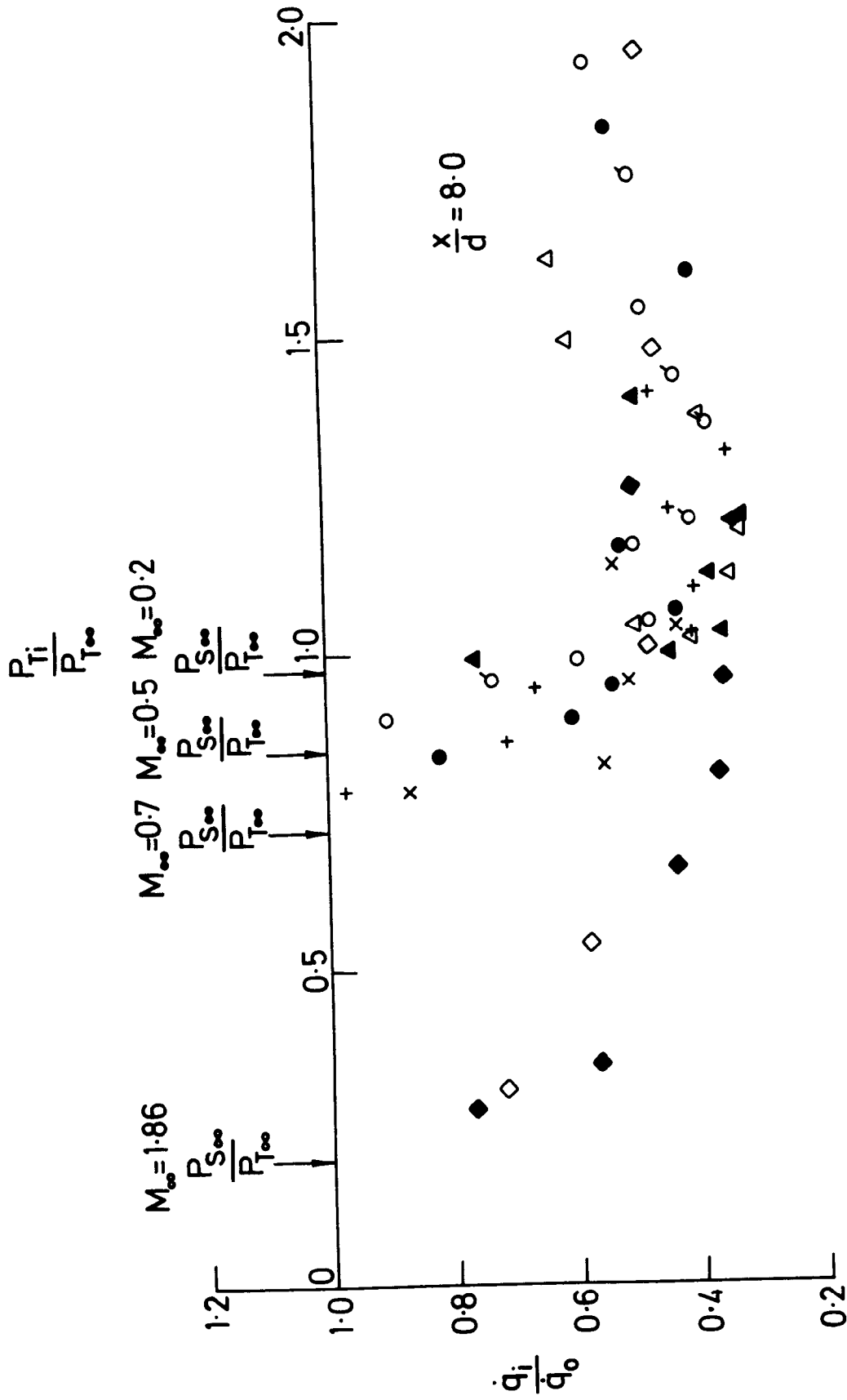
1 row at $30^\circ \frac{x}{d} = 8.0$

Figure 20. Graph of $\dfrac{q_i}{q_o}$ against $\dfrac{P_{Ti}}{P_{T\infty}}$, all Mach numbers.
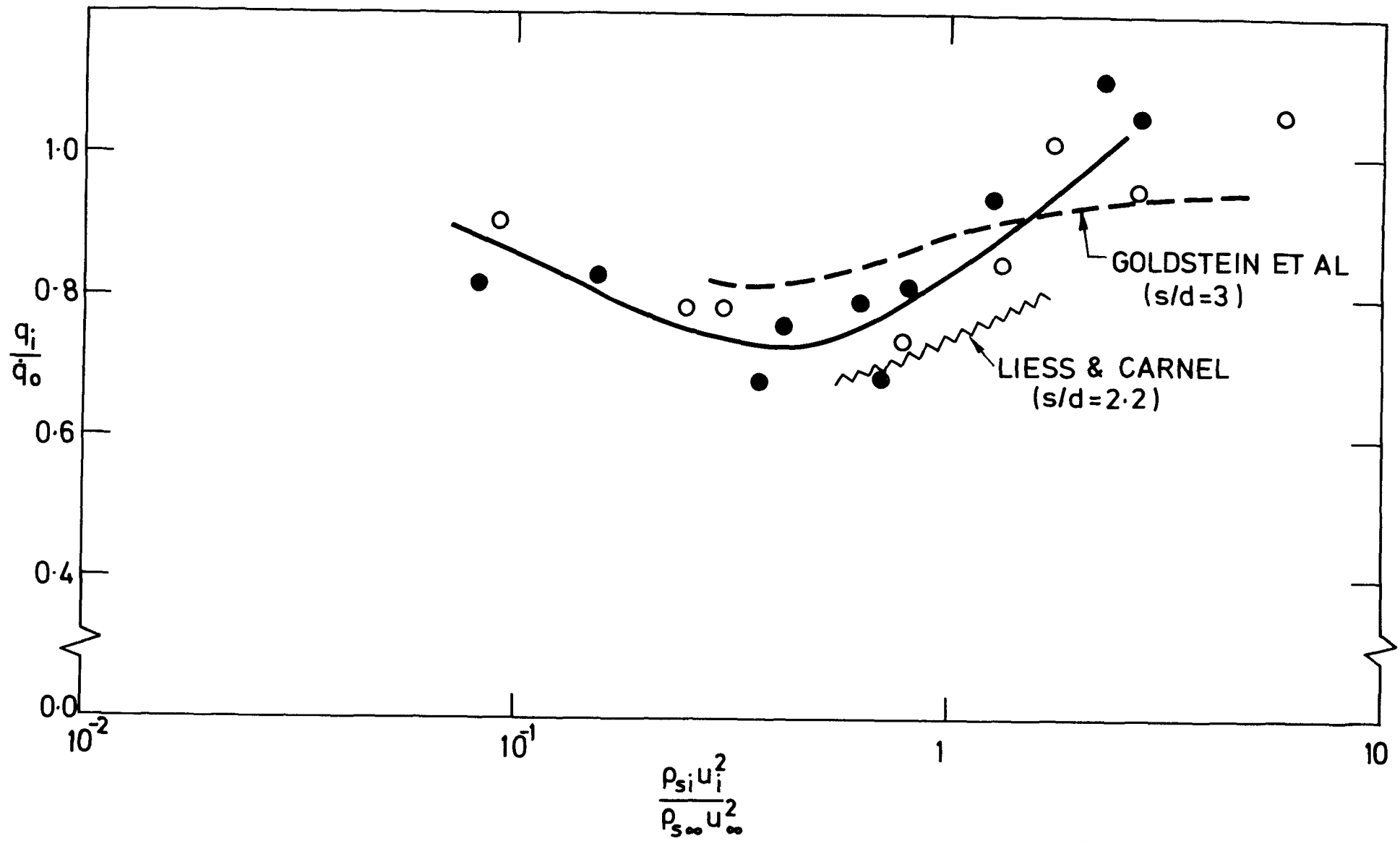
Figure 21. Comparison of data with that of other workers, plotted as $\dfrac{\dot{q}_i}{\dot{q}_o}$

against $\dfrac{\rho_{si}u_i^2}{\rho_{s\infty}u_\infty^2}$.   1 row at 30° $\dfrac{x}{d}$ = 10.
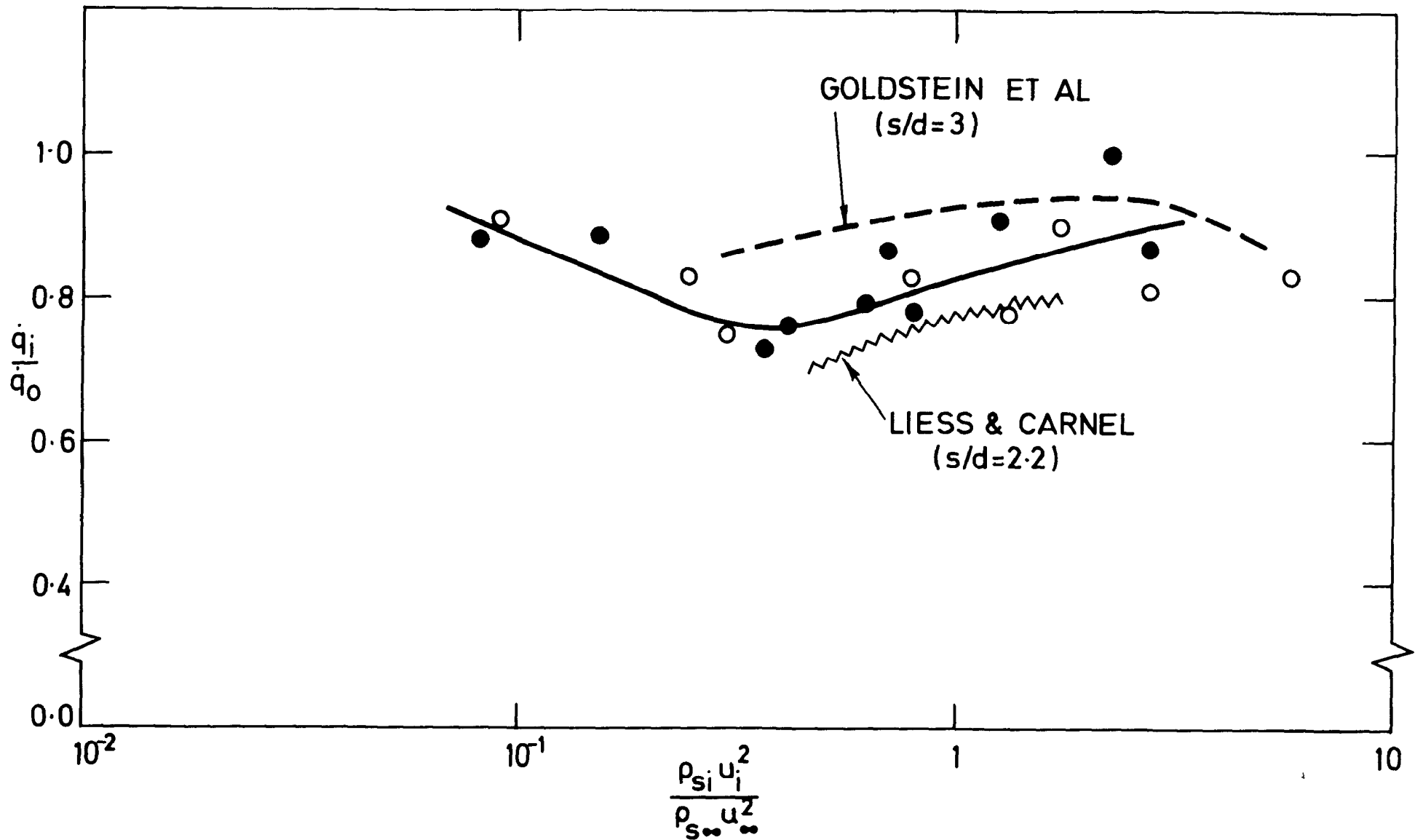
Figure 22. Comparison of data with that of other workers, plotted as $\dfrac{\dot{q}_i}{\dot{q}_o}$ against $\dfrac{\rho_{si} u_i^2}{\rho_{s\infty} u_\infty^2}$. 1 row at 30° $\dfrac{x}{d} = 25$.
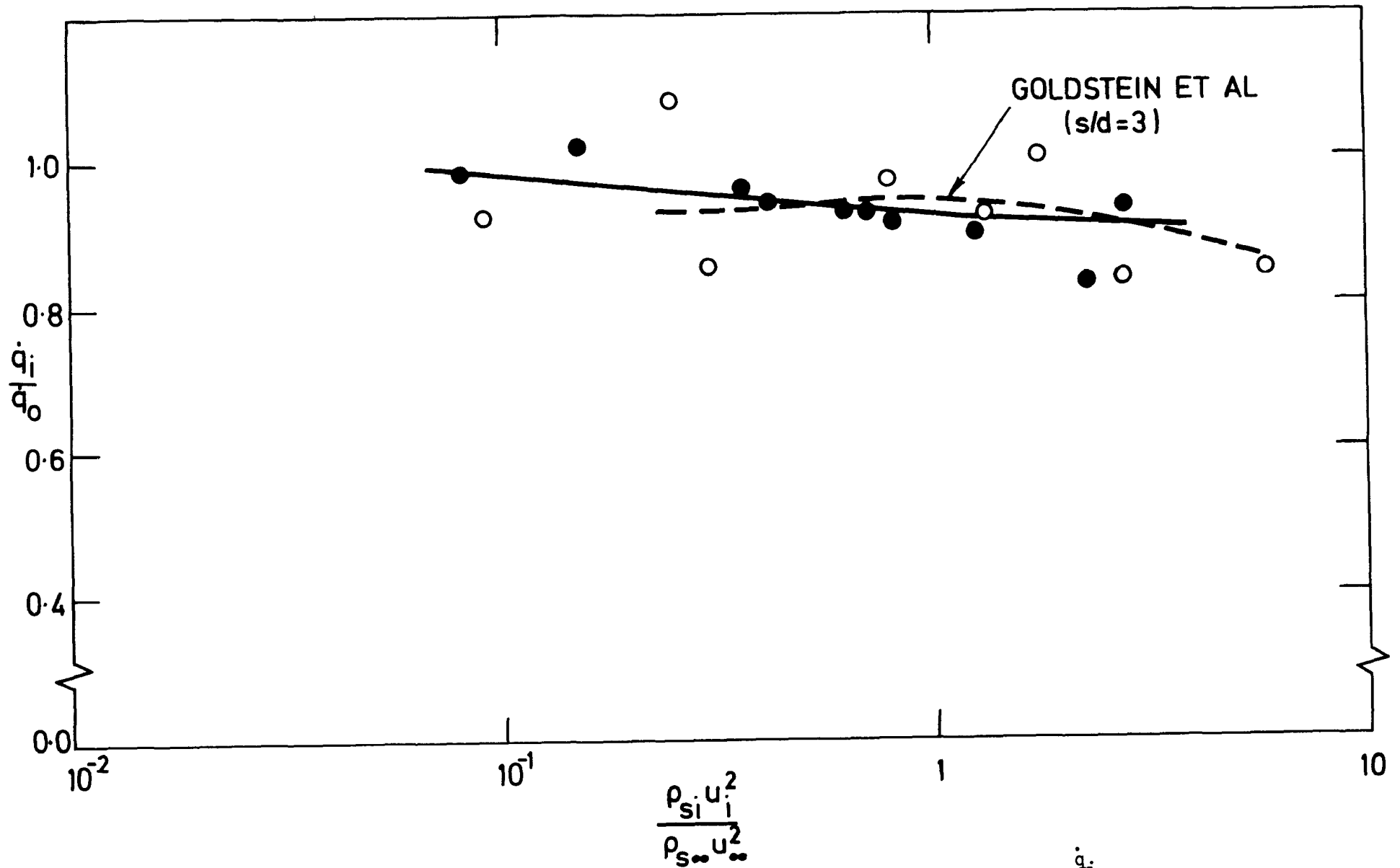
Figure 23.   Comparison of data with that of other workers, plotted as $\dfrac{\dot{q}_i}{\dot{q}_o}$ against $\dfrac{\rho_{si} u_i^2}{\rho_{s\infty} u_\infty^2}$. 1 row at $30°$, $\dfrac{x}{d} = 80$.
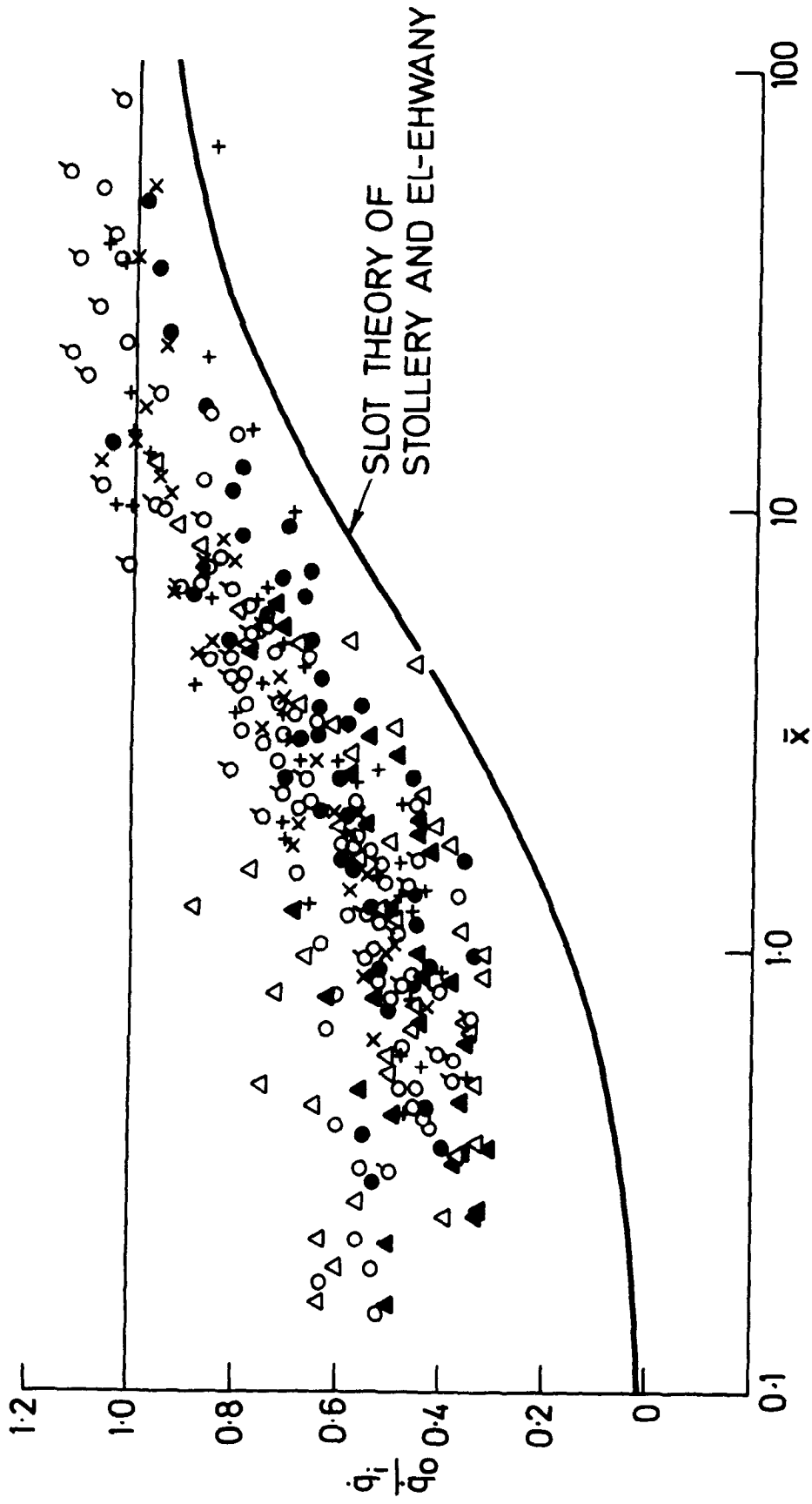
Figure 24(a). Graph of $\frac{\dot{q}_i}{\dot{q}_o}$ against $\bar{x}$. 2 rows at $90°$.
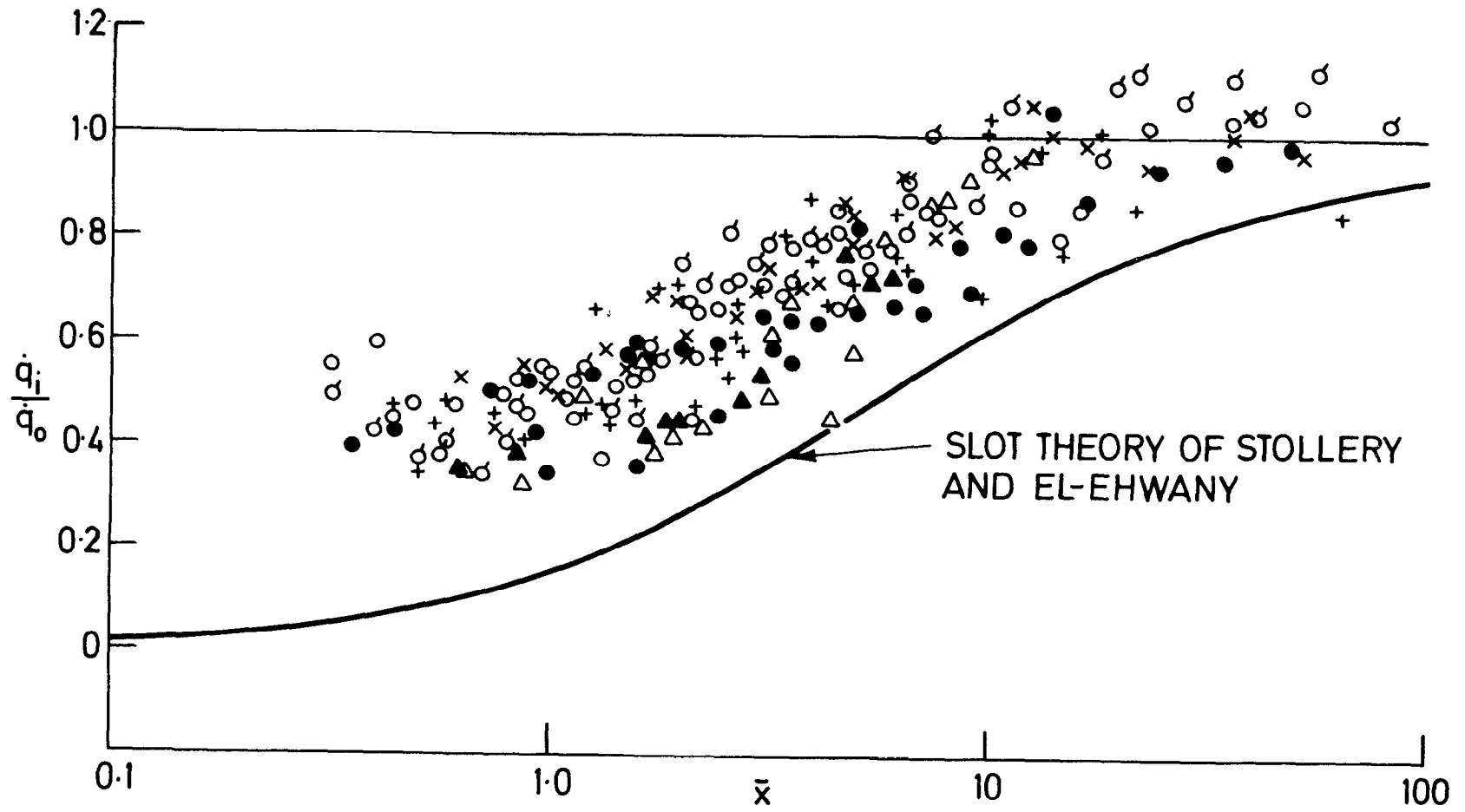
Figure 24(b). Graph of $\frac{\dot{q}_i}{\dot{q}_o}$ against $\bar{x}$. 2 rows at $90°$. Points for which $\dfrac{\rho_{si} u_i^2}{\rho_{s\infty} u_\infty^2} > 3.0$ removed.
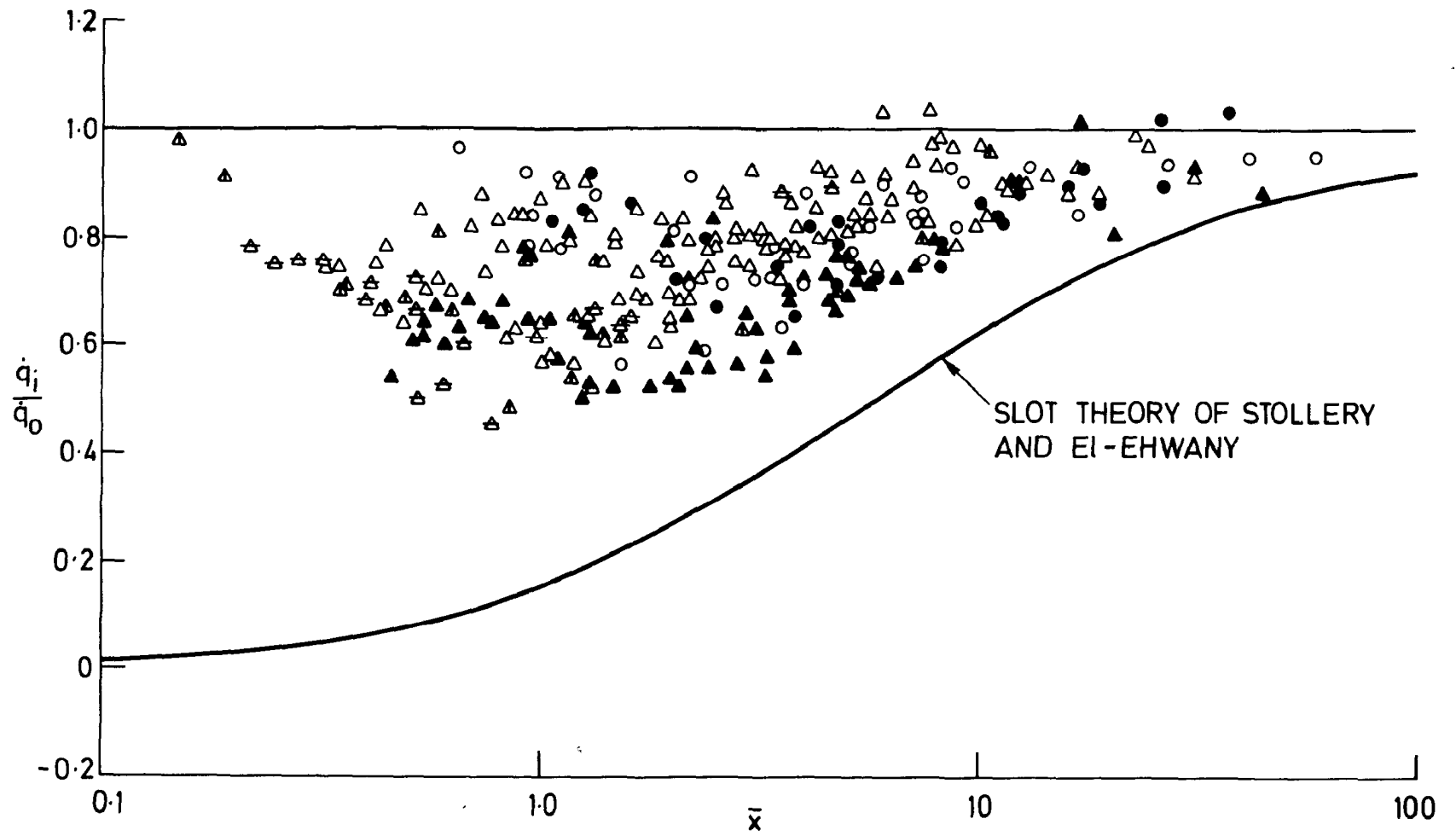
Figure 25(a).   Graph of $\dfrac{\dot{q}_i}{\dot{q}_o}$ against $\bar{x}$.   1 row at 90°.
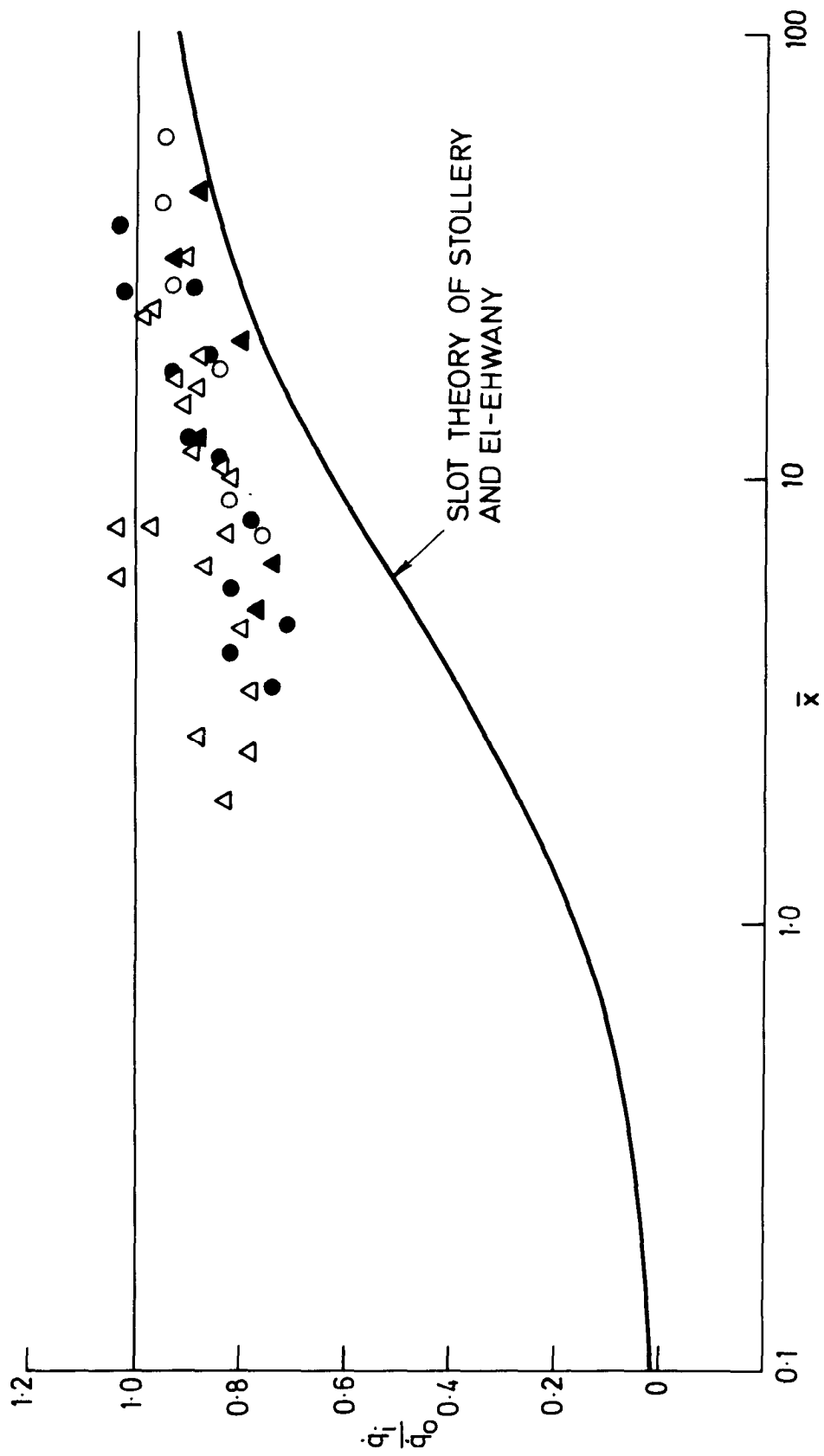
Figure 25(b). Graph of $\dfrac{\dot{q}_i}{\dot{q}_o}$ against $\bar{x}$. 1 row at 90°. Points for which

$$\dfrac{\rho_{si}u_i^2}{\rho_{s\infty}u_\infty^2} > 1.0 \text{ removed.}$$
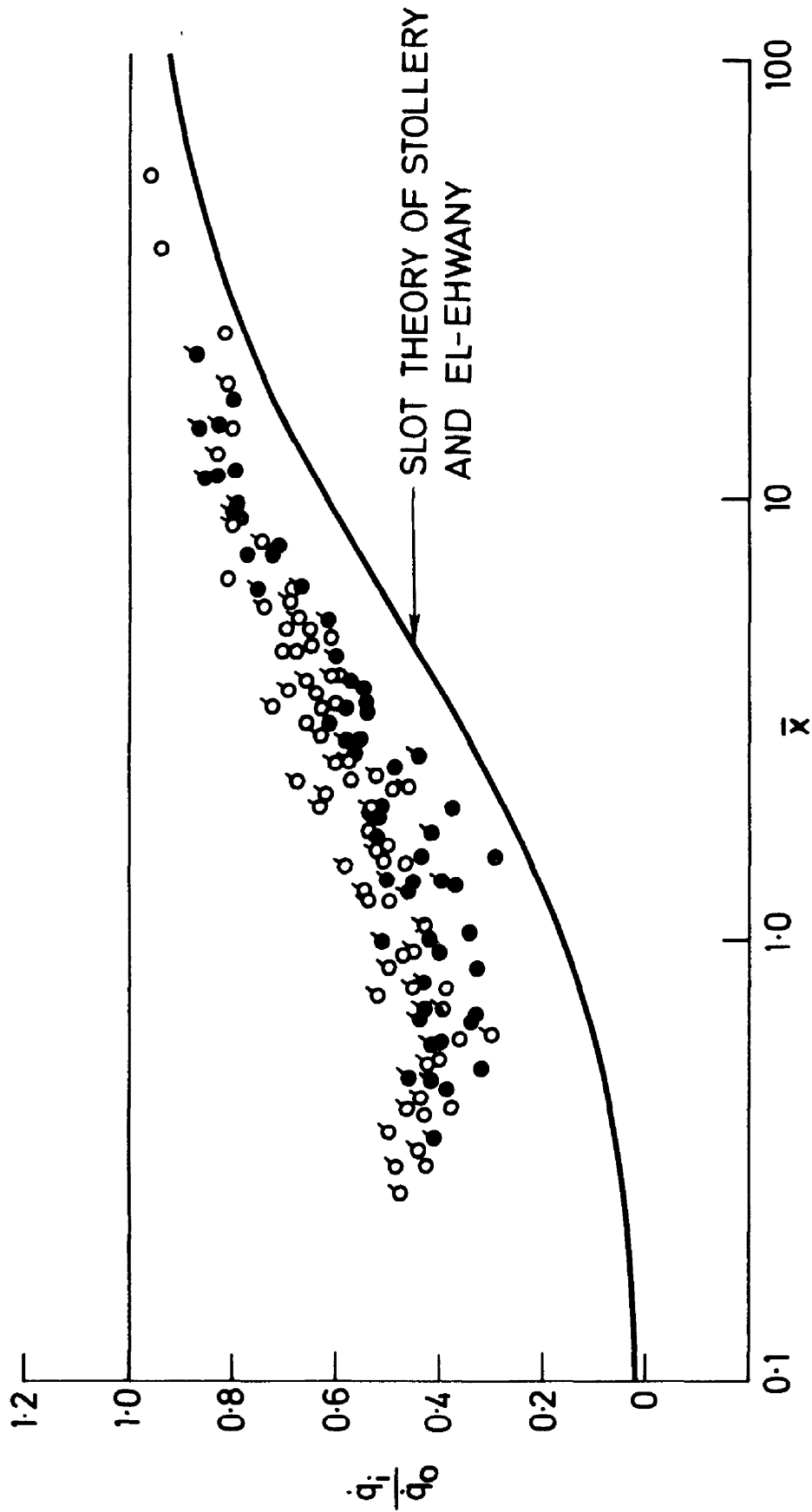
Figure 26. Graph of $\frac{\dot{q}_i}{\dot{q}_o}$ against $\bar{x}$. 2 rows at $30°$.
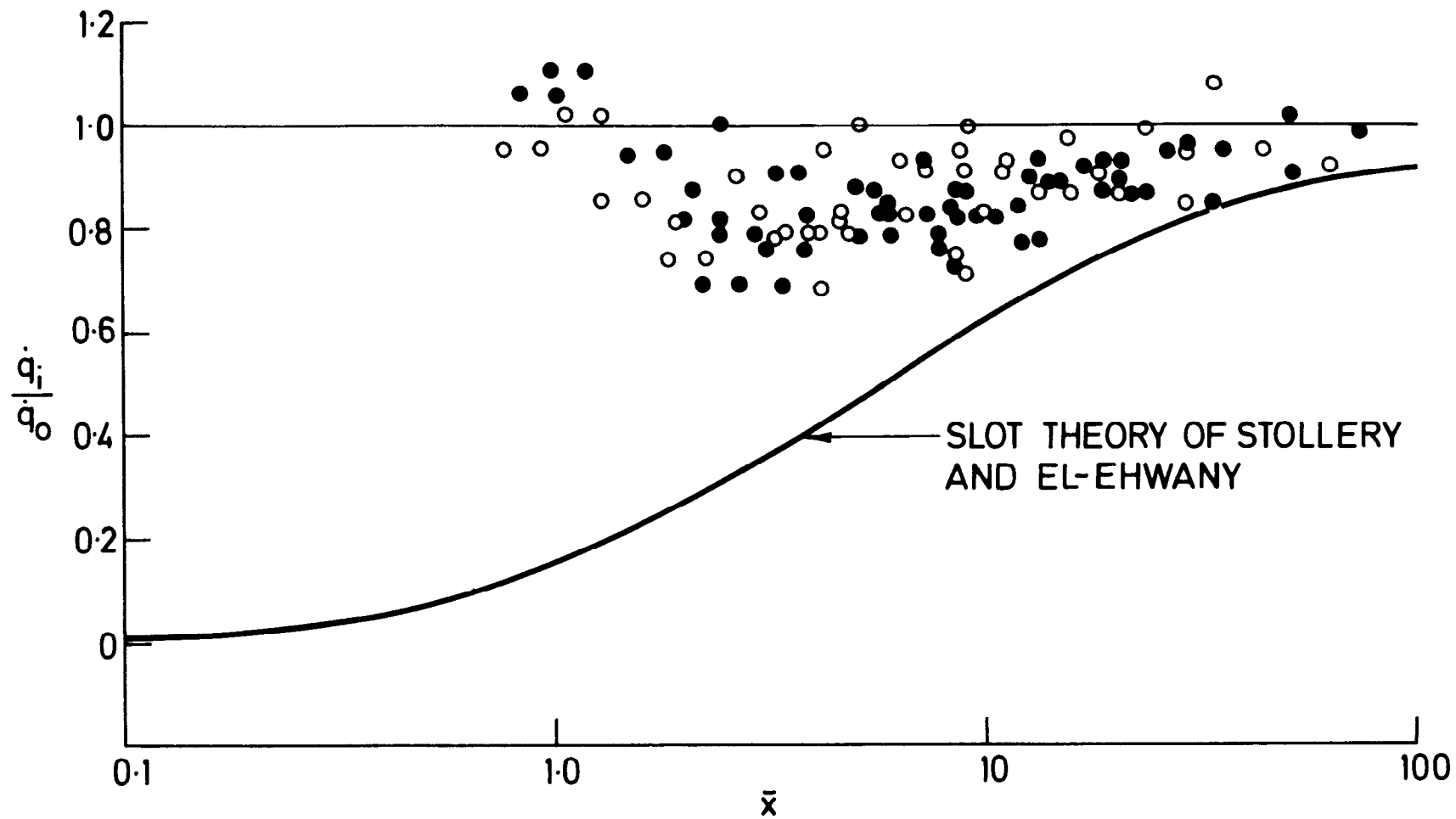
Figure 27. Graph of $\dfrac{\dot{q}_i}{\dot{q}_o}$ against $\bar{x}$. 1 row at 30°.
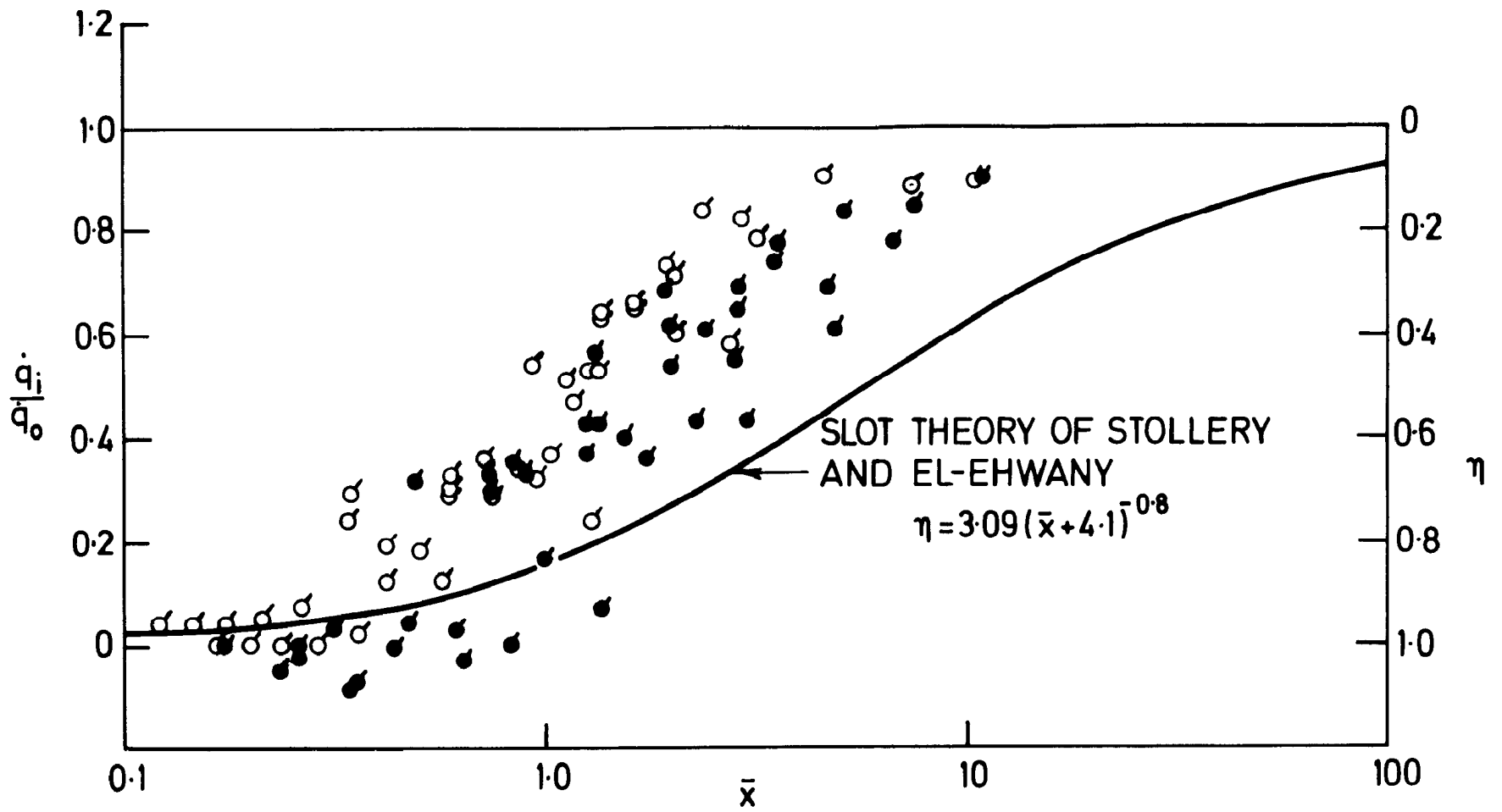
Figure 28.   Graph of $\dfrac{\dot{q}_i}{\dot{q}_o}$ against $\bar{x}$.   Slot at $30°$.

Figure 29.   Graphs of $\dfrac{\dot{q}_i}{\dot{q}_o}$ against $\dfrac{P_{Ti}}{P_{T\infty}}$ for four values of $\dfrac{x}{d}$.   Slot at $30°$.
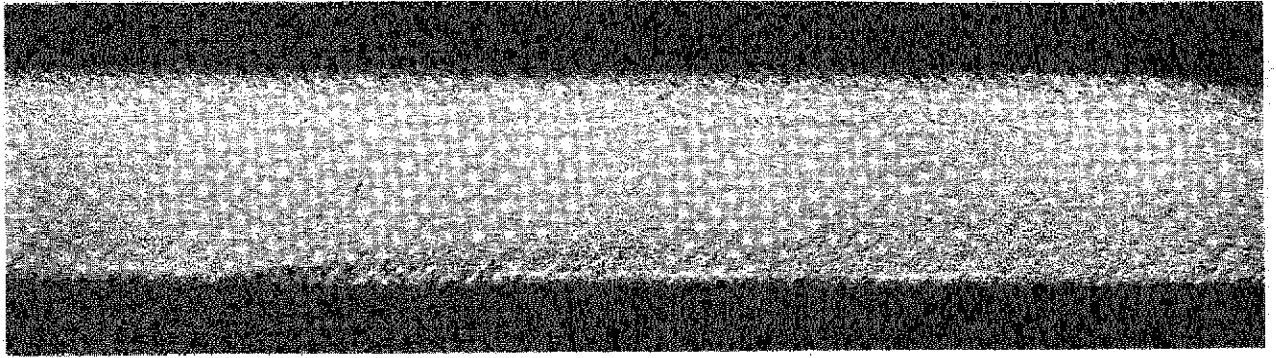
(a) $\dfrac{P_{Ti}}{P_{T\infty}} = 0.89$
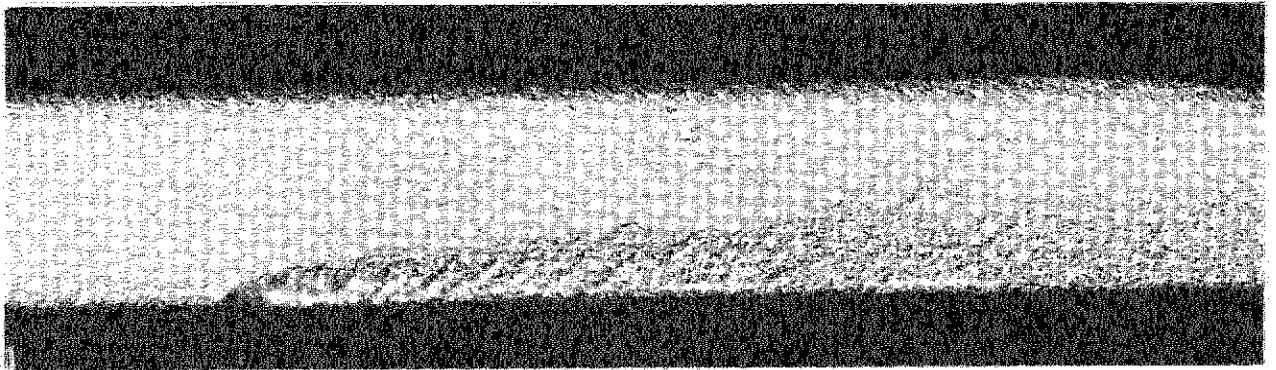
(b) $\dfrac{P_{Ti}}{P_{T\infty}} = 1.21$
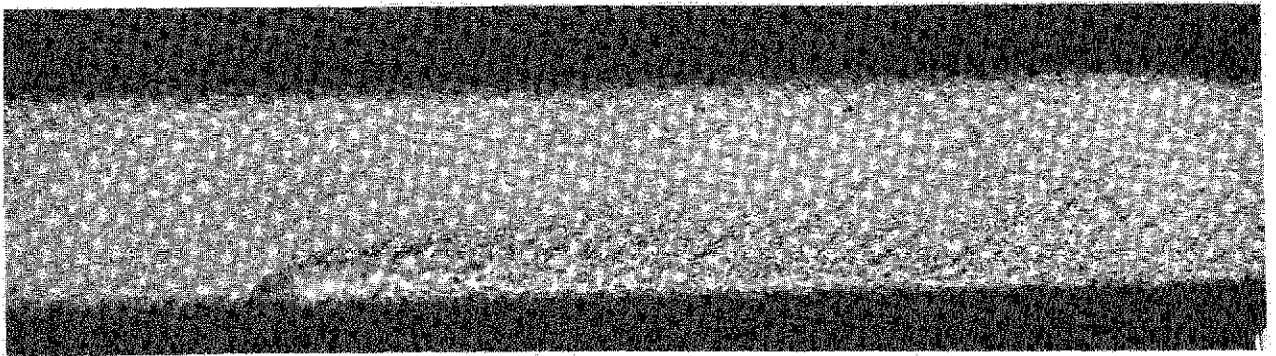
(c) $\dfrac{P_{Ti}}{P_{T\infty}} = 1.79$

Plate 1. Shadowgraphs showing flow with injection. $M = 0.5$, 2 rows at 90°
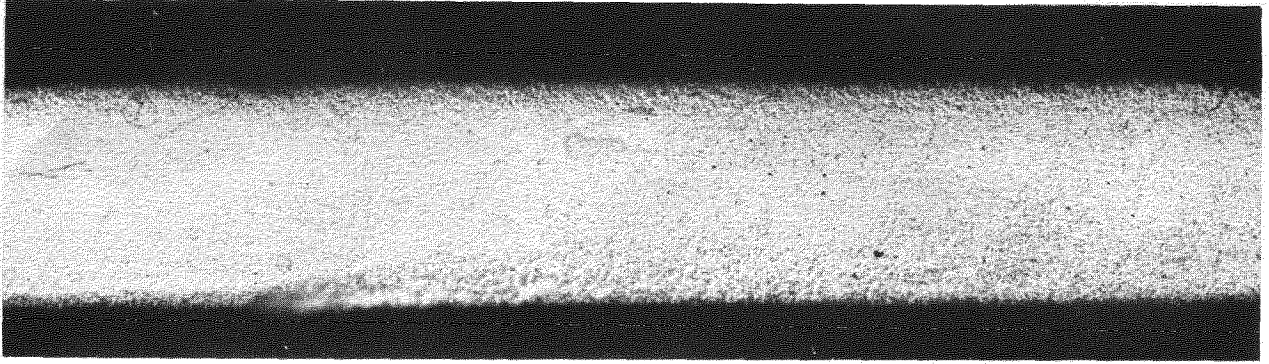
(a) $\dfrac{P_{Ti}}{P_{T\infty}} = 1.02$
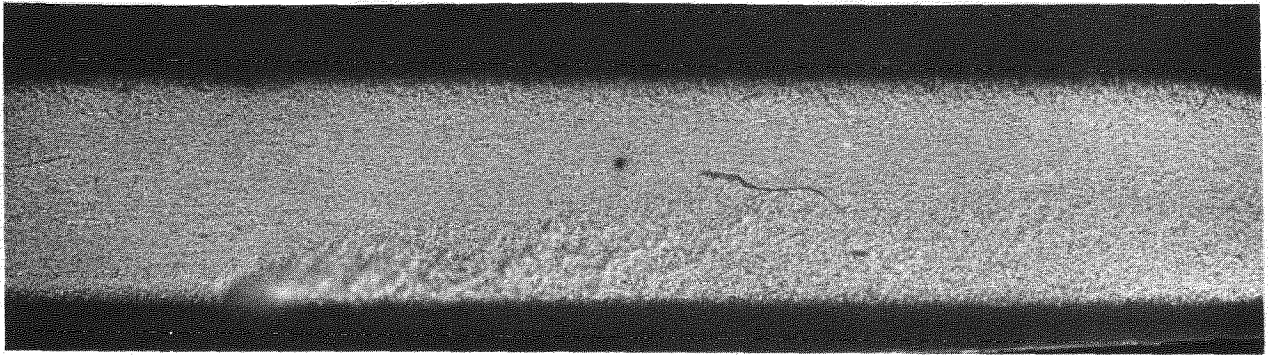
(b) $\dfrac{P_{Ti}}{P_{T\infty}} = 1.19$
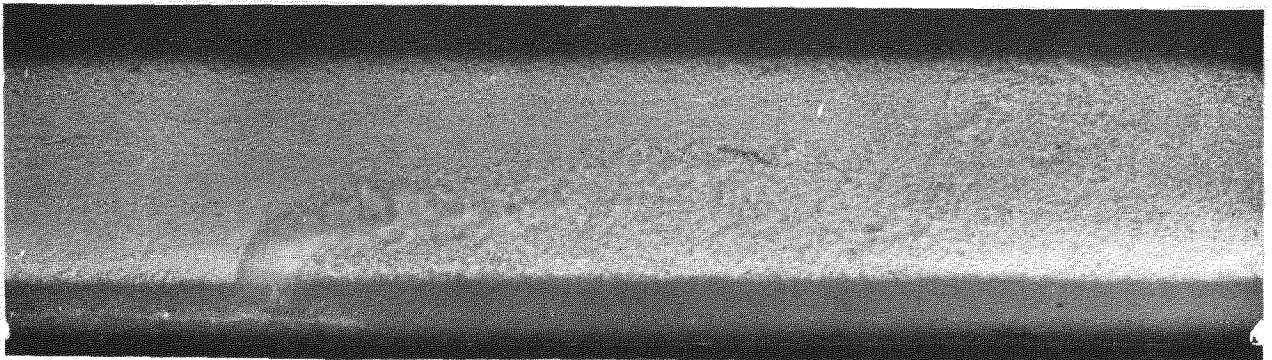
(c) $\dfrac{P_{Ti}}{P_{T\infty}} = 1.49$

Plate 2. $M_\infty = 0.2$, 2 rows at 90°. Note the more abrupt onset of "Lift-off compared with Plate 1.
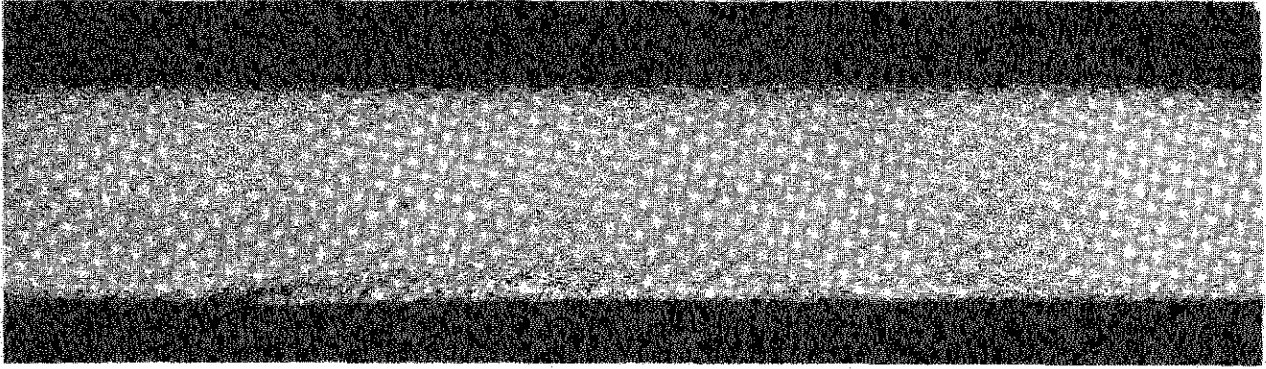
(a) $\dfrac{P_{Ti}}{P_{T\infty}} = 0.86$
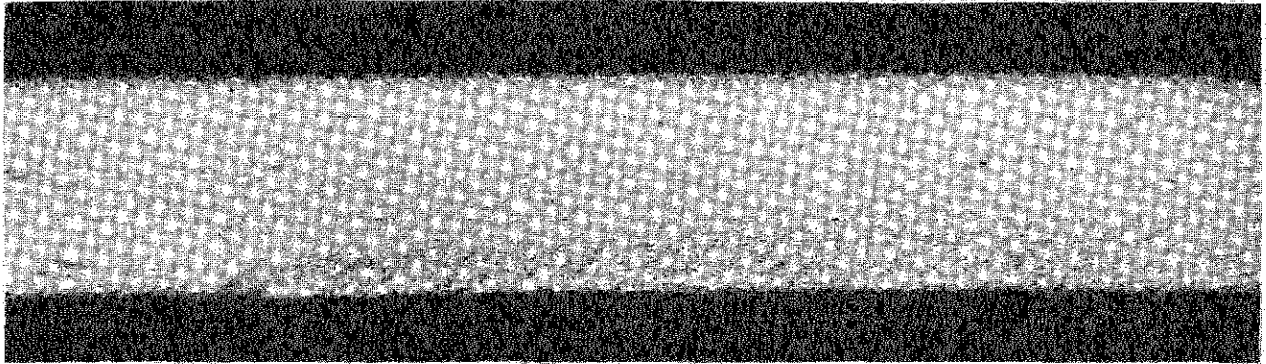
(b) $\dfrac{P_{Ti}}{P_{T\infty}} = 1.22$
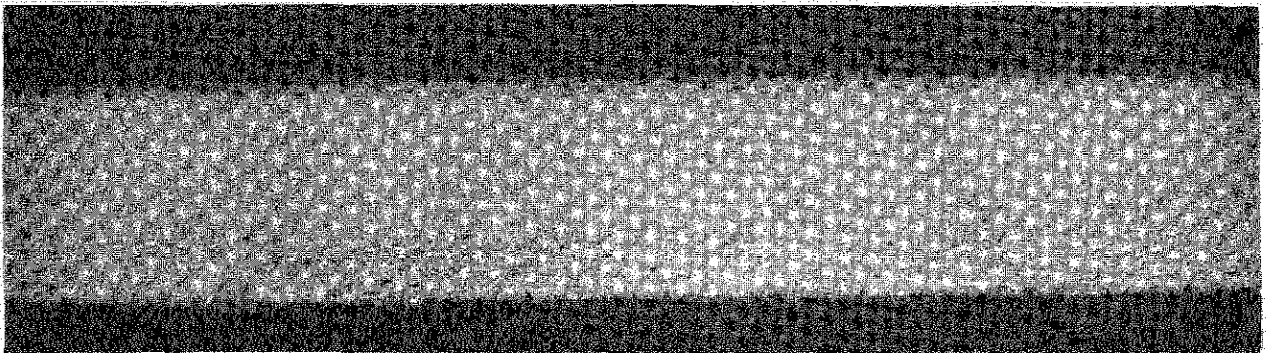
(c) $\dfrac{P_{Ti}}{P_{T\infty}} = 1.41$

Plate 3. $M_\infty = 0.7$, 2 rows at 90°. "Lift-off" is less apparent than at the lower Mach numbers in Plates 1 and 2.
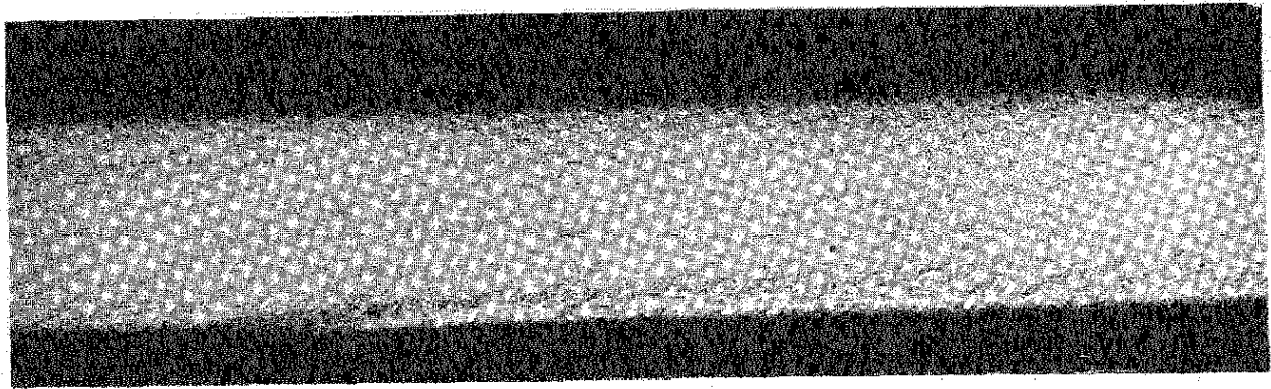
(a) $\dfrac{P_{Ti}}{P_{T\infty}} = 0.90$
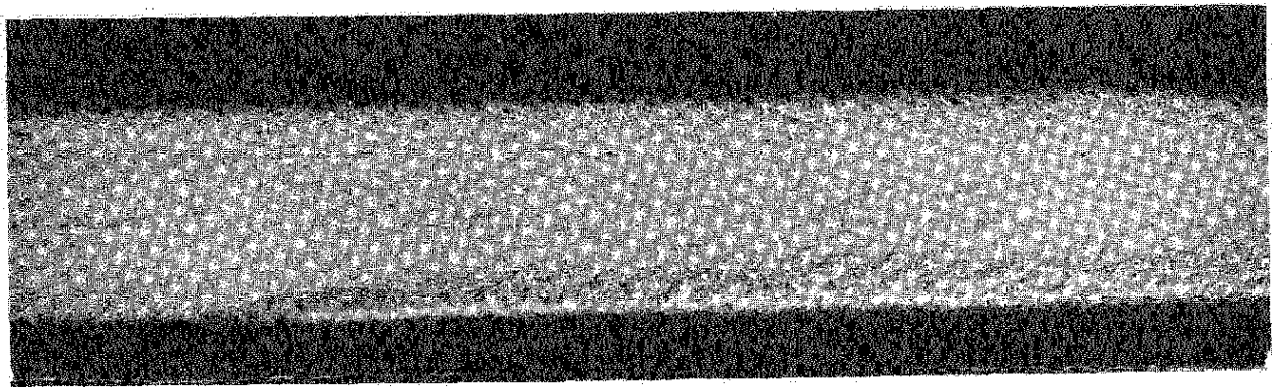
(b) $\dfrac{P_{Ti}}{P_{T\infty}} = 1.22$
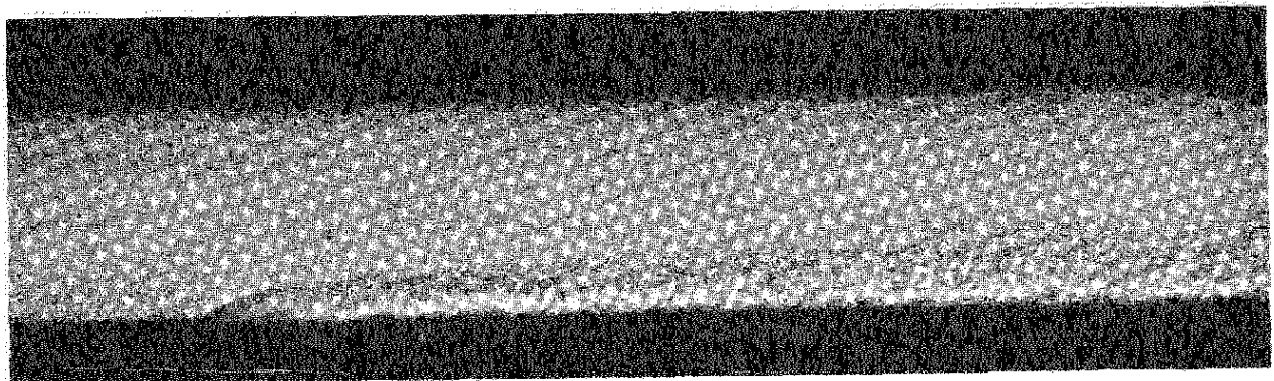
(c) $\dfrac{P_{Ti}}{P_{T\infty}} = 1.57$

Plate.4. $M_{\infty} = 0.5$, 2 rows at 30°. "Lift-off" is less severe than for 90° holes under the same conditions, as in Plate 1.
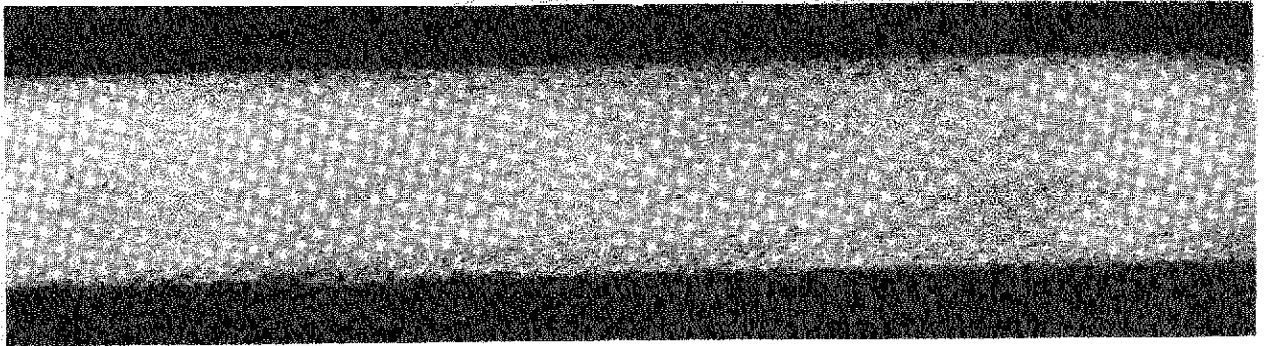
(a) $\dfrac{P_{Ti}}{P_{T\infty}} = 0.96$
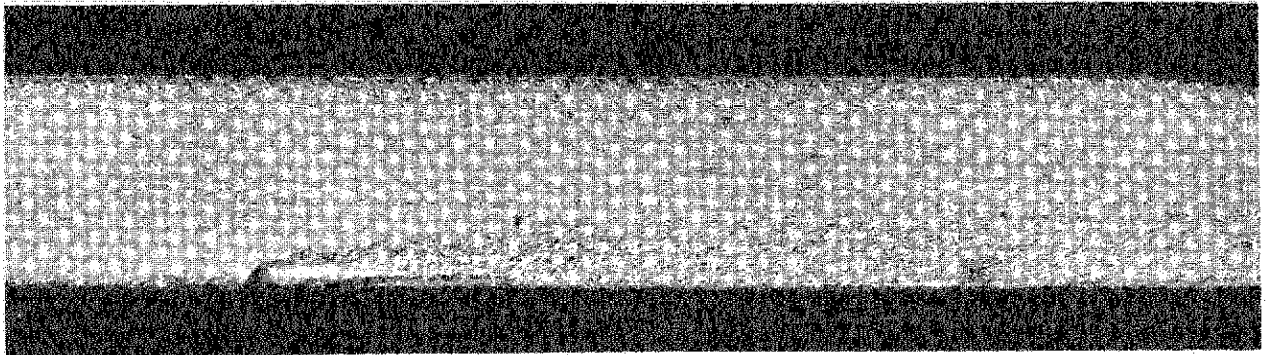
(b) $\dfrac{P_{Ti}}{P_{T\infty}} = 1.36$
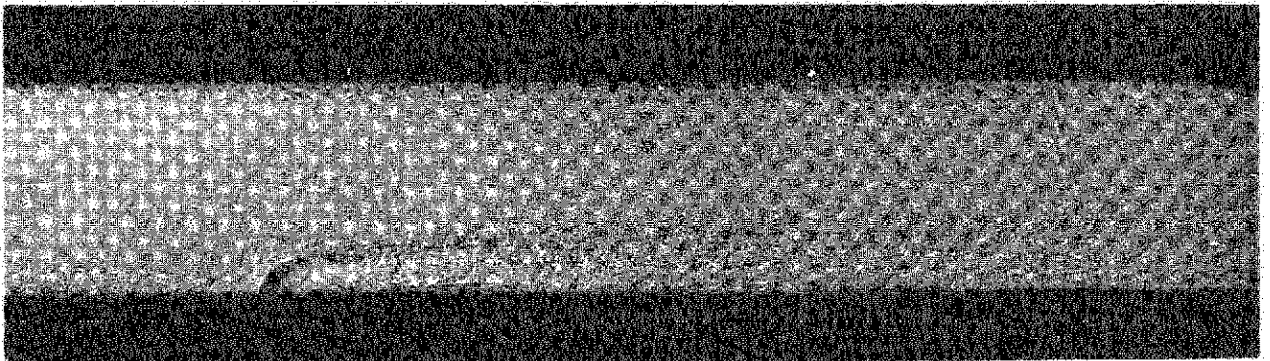
(c) $\dfrac{P_{Ti}}{P_{T\infty}} = 1.70$

Plate 5. $M_\infty = 0.5$, 1 row at 90°. "Lift-off" is more marked than in the case of a 2 row geometry, Plate 1.
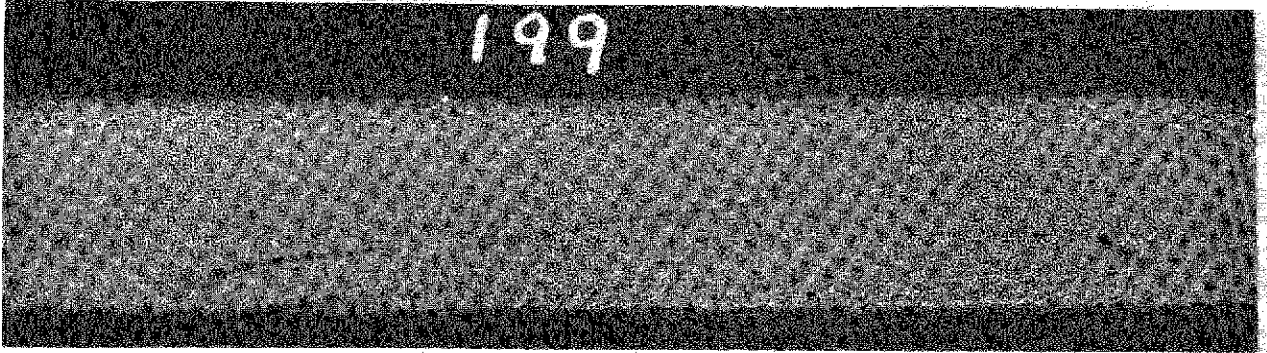
(a) $\dfrac{P_{Ti}}{P_{T\infty}} = 0.95$
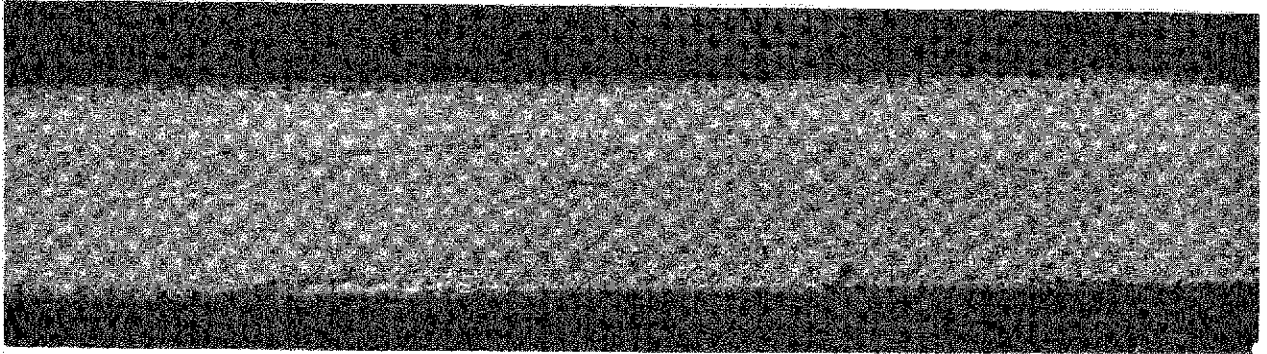
(b) $\dfrac{P_{Ti}}{P_{T\infty}} = 1.26$
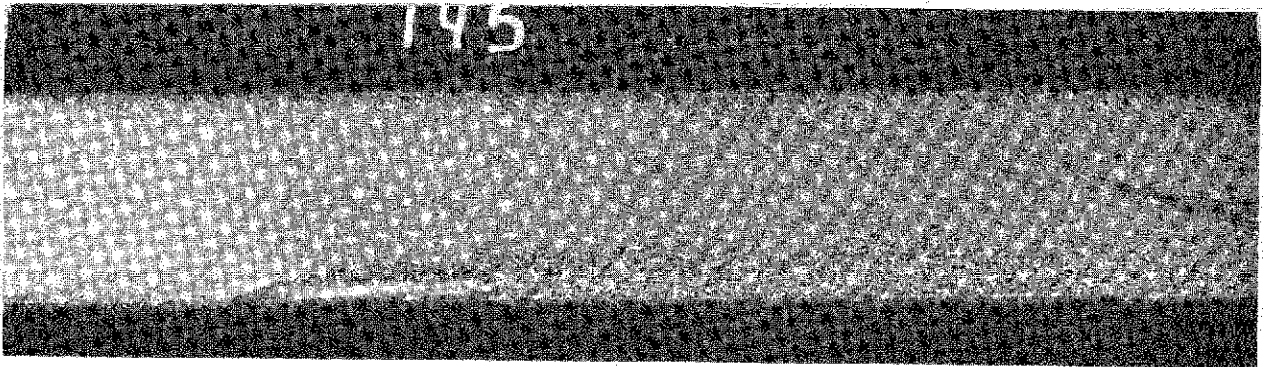
(c) $\dfrac{P_{Ti}}{P_{T\infty}} = 1.85$

Plate 6. $M_{\infty} = 0.5$, 1 row at 30°.
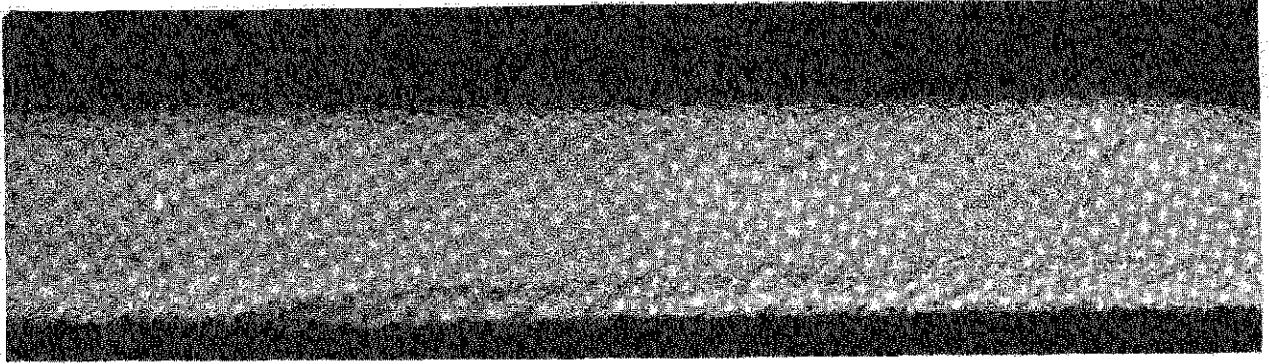
(a) $\dfrac{P_{Ti}}{P_{T\infty}} = 0.914$
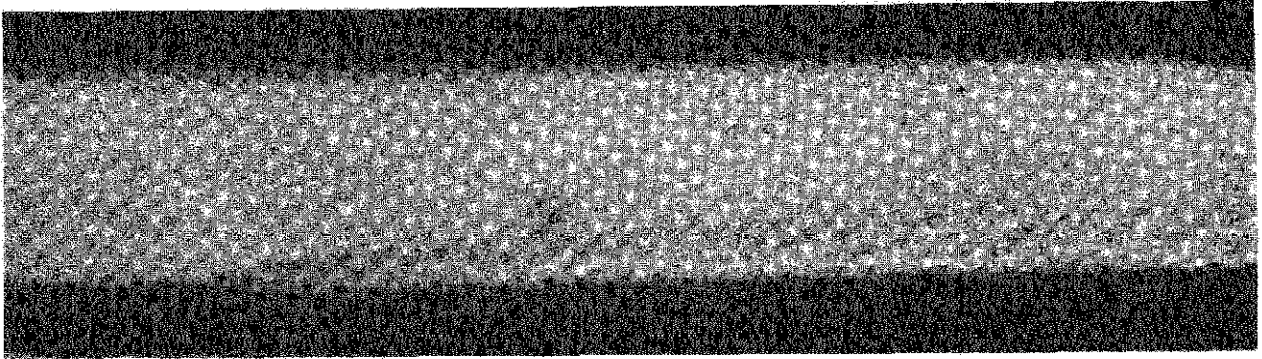
(b) $\dfrac{P_{Ti}}{P_{T\infty}} = 1.07$
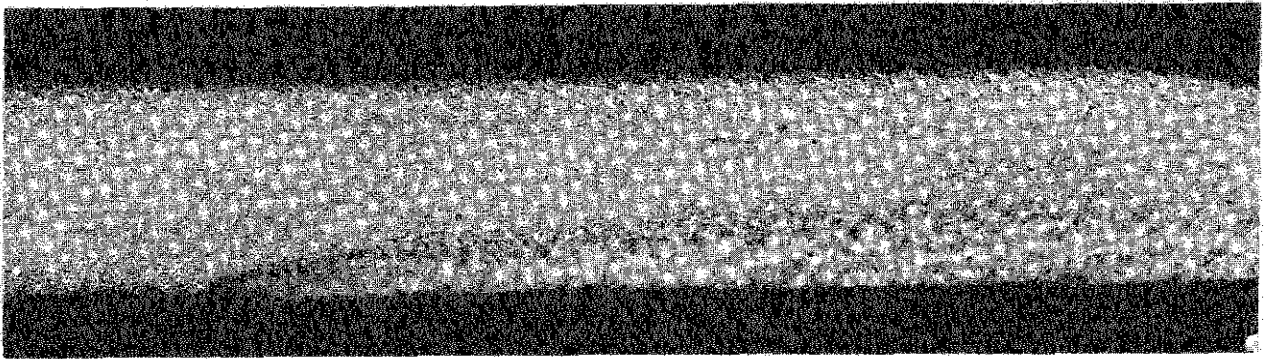
(c) $\dfrac{P_{Ti}}{P_{T\infty}} = 1.53$

Plate 7. $M_\infty = 0.5$, slot at 30°. "Lift-off" is much reduced compared with any

of the hole geometries.

typical of those found in gas turbines are thus within
the range of the experimental conditions.

The experimental results are analysed using the
boundary layer film cooling model parameter $\bar{x}$ and the
mass and momentum flux ratios as correlating parameters.
The latter gives good correlation of the experimental
data, and a useful comparison with data obtained by
other workers under different conditions. The
correlated data may also be used as a prediction for film
cooling in any situation, and as a test for new
theoretical models of the film cooling process.

DETACHABLE AB

ARC CP No.1303
December 1973
Smith, M.R., Jones, T.V. and Schultz, D.L.

FILM COOLING EFFECTIVENESS FROM ROWS OF HOLES
UNDER SIMULATED GAS TURBINE CONDITIONS

Experiments are reported in which film cooling tests
are carried out using coolent injection through rows of
discrete holes. A shock tunnel is used to provide a
transient mainstream flow at stagnation temperatures of
500°K, 1000°K and 2000°K. Wall heat transfer rates are
measured with and without coolant injection using thin
film gauges. Mainstream Mach numbers of 0.2, 0.5 and
0.7 are employed. Mach numbers, Reynolds numbers,
gas-to-wall temperature ratios and flow temperatures

typical/